III.Results and Discussion

1. Preparation of PU-Organoclay Hybrid

The synthesis of new organic–inorganic nanocomposite materials was achieved by the intercalation of polyurethane onto functionalized montmorillonite clay through *in-situ* polycondensation polymerization technique. PU/organoclay nanocomposites were synthesized through the intercalation of diols and/or diamine into organoclay interlayers followed by the addition of **TDI** to produce the intercalated polyurethanes through two steps as illustrated in **Schemes 2-4**. The first step is the modification of hydrophilic clay to become organophilic to promote the absorption of organic materials used in the formation of **PU** into the interlayer spacing to improve the particle-matrix interactions. This step was achieved through ion exchange process between sodium cations in MMT and ammonium salt of tyramine or ammonium salt of aminolauric acid ($\mathbf{I}_{a,\ b}$). The presence of reactive function groups in the modified clay allows the clay to react with diisocyanate. The calcination of organoclays indicates the modification was achieved with a high degree of conversion of 88% and 86% for $\mathbf{I}_a$ and $\mathbf{I}_b$, respectively.

The second step for the formation of polyurethane-clay nanocomposites by the dispersion of the organoclay in a solution of diol and diamine in **DMF**. It was found that the modified clay was dispersed easily in the diol and diamine at room temperature. This step was followed by adding **TDI** to produce the intercalated polyurethanes $\mathbf{III}_{a\text{-}f}$ and $\mathbf{V}_{a\text{-}e}$ through *in-situ* polycondensation polymerization technique. The produced hybrid films ($III_{a\text{-}f}$, $V_{a\text{-}e}$) are transparent or semi-transparent depending on the organoclay content.

Another series of PU–organoclay nanocomposites were synthesized through several steps as illustrated in **Schemes 5-7**. The first step was the preparation of vinyl monomer-containing ammonium salt by quaterization of

N,N-dimethyl-*n*-octadecylamine with 4-vinylbenzyl chloride to produce *N,N*- dimethyl-N-(4-vinylbenzyl)-n-octadecyl ammonium chloride salt.

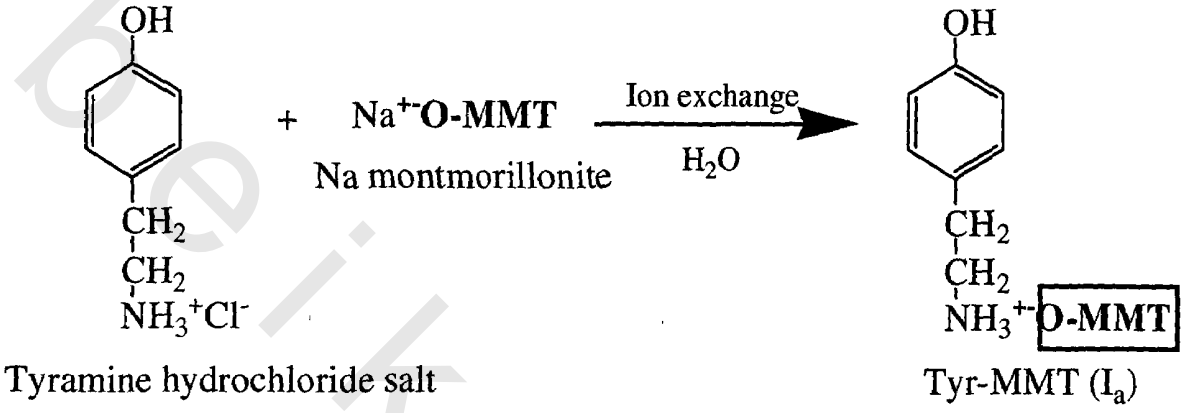

Tyramine hydrochloride salt

Tyr-MMT (I_a)

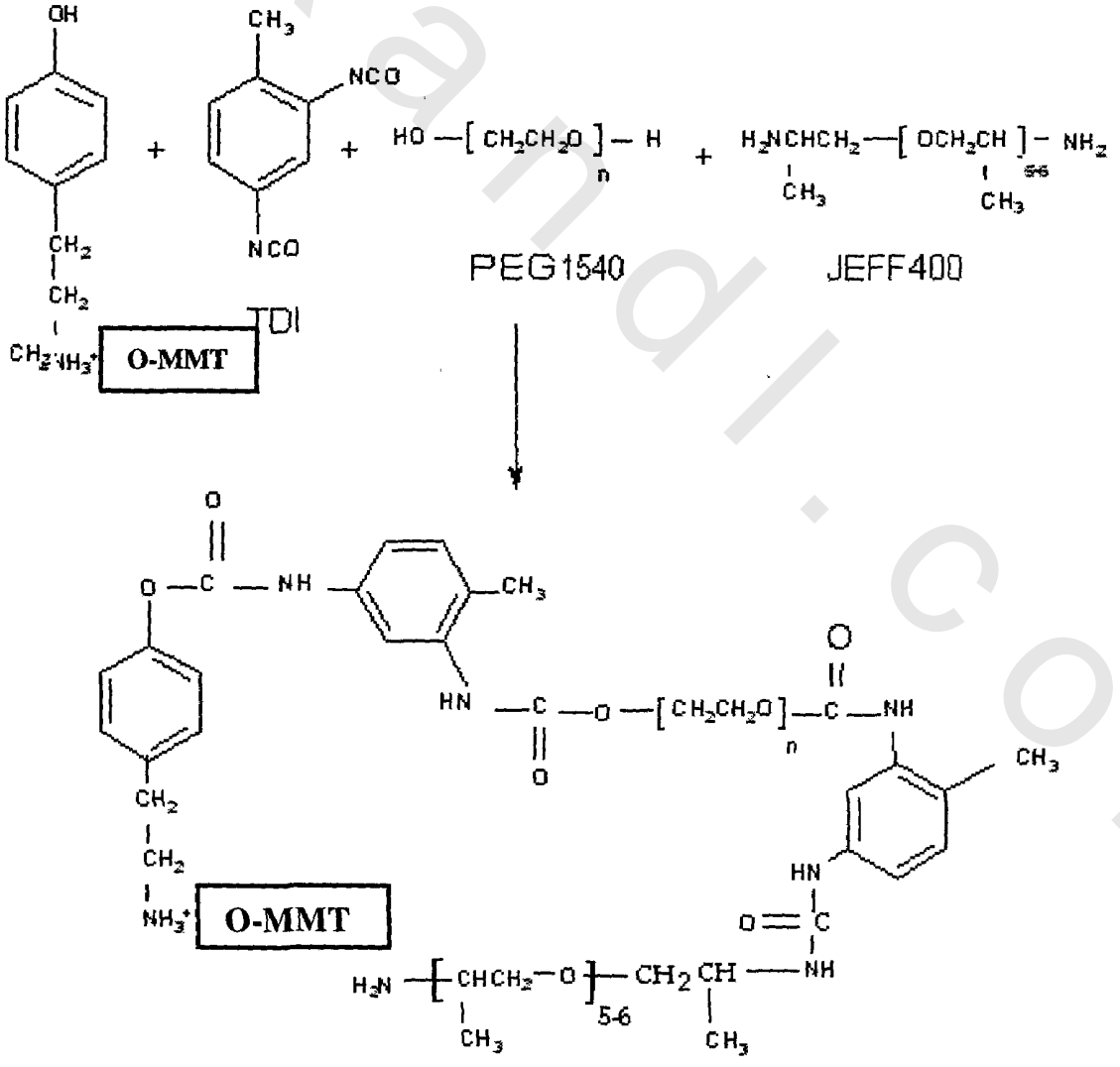

Scheme 2: Preparation of PU/Tyr-MMT composites III_{a-f}

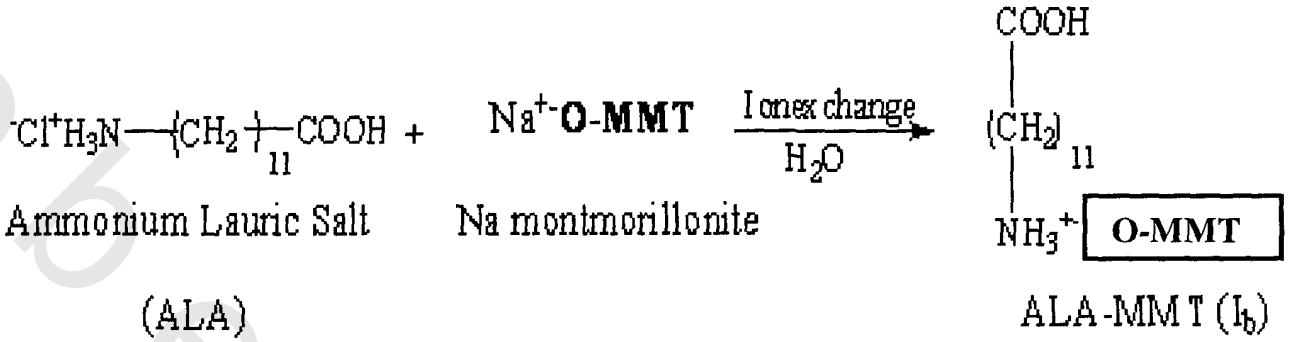

(ALA)

ALA-MMT (I_b)

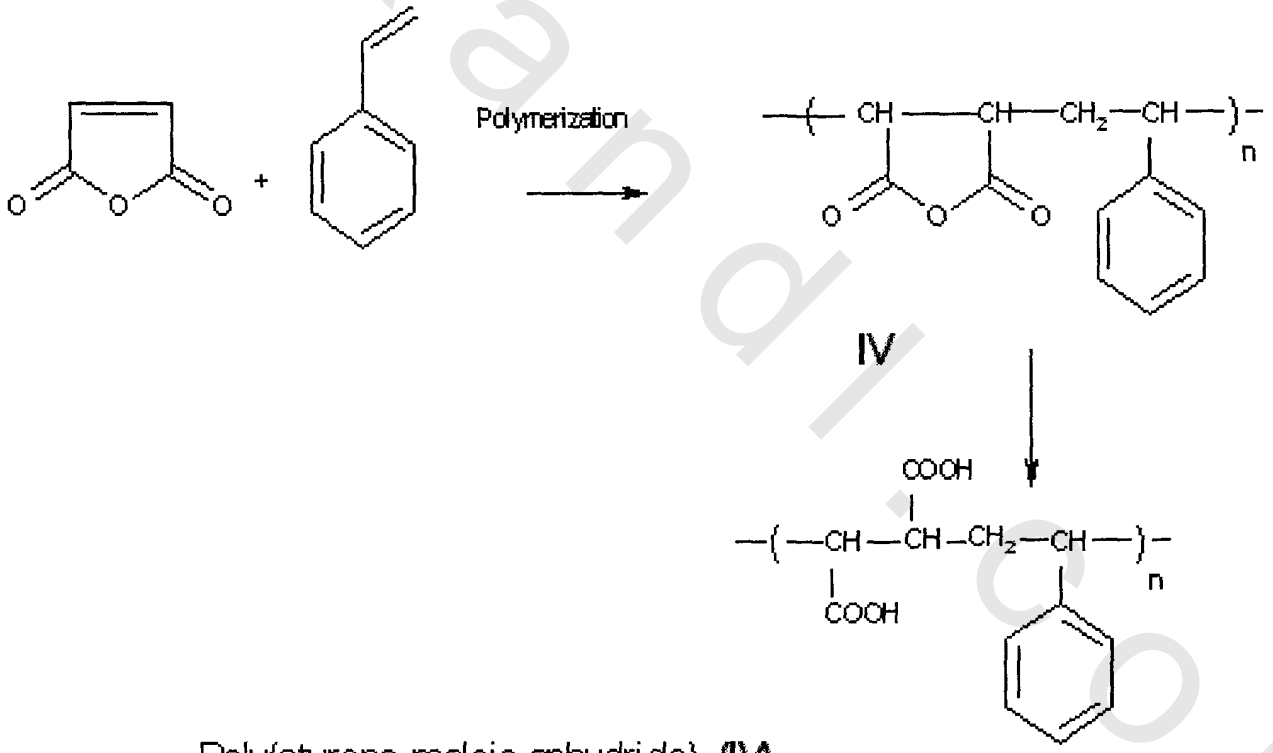

Poly(styrene-maleic anhydride) **(IV)**

Scheme 3: Preparation of $\mathbf{I_b}$ and PSMA **(IV)**

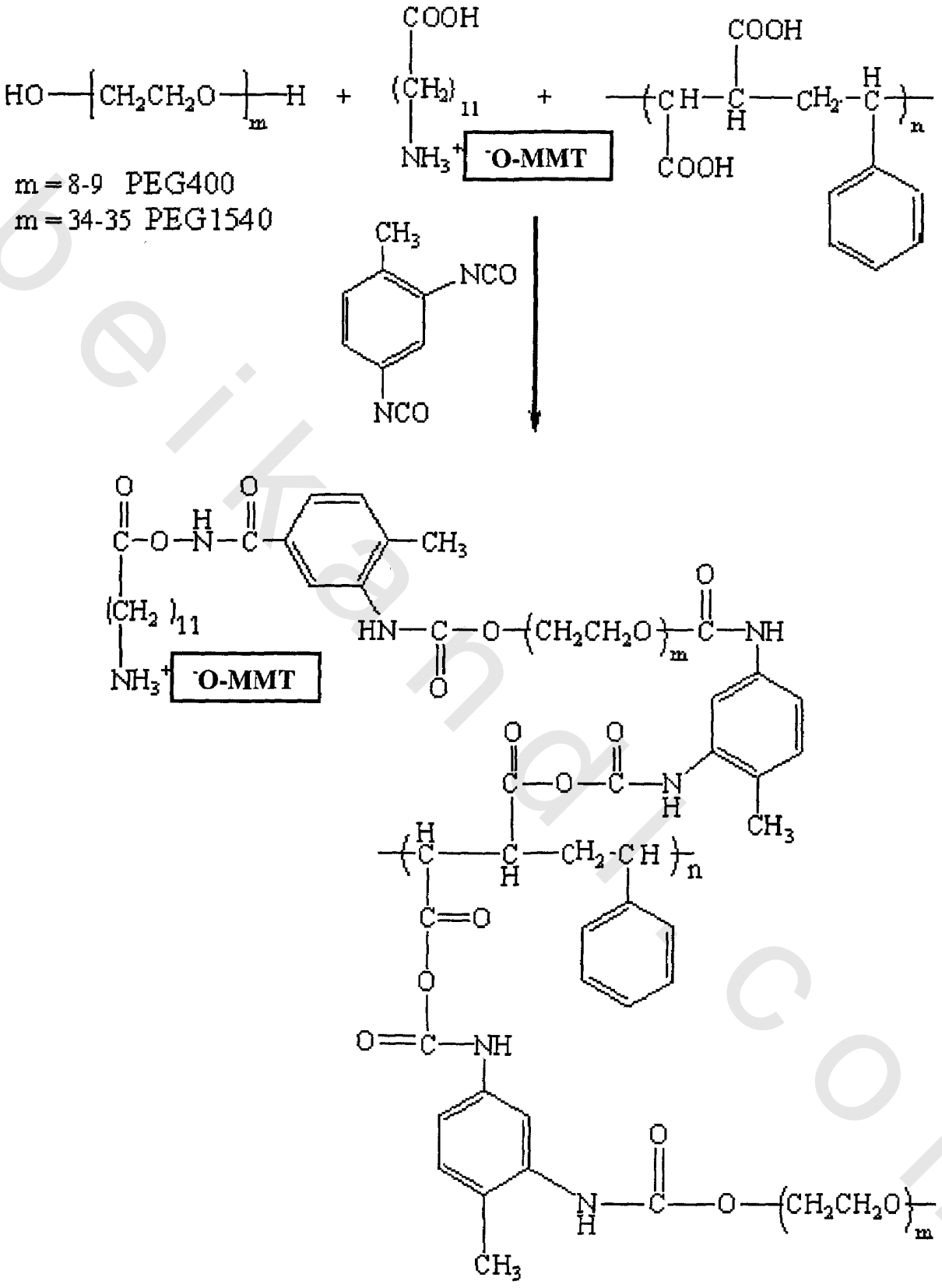

V_{a-e}

Scheme 4: Preparation of PU-MMT composites V_{a-e}

The ^{1}**H-NMR** spectra **Figure 6** and data were recorded for vinyl monomers **II** in which the **H** of chloromethyl group (CH_2Cl) was shifted from 4.6 ppm for **CMS** to 5.3 ppm corresponding to the quaternary salt to 4.2 ppm for **II.** The peaks at 5.0, 5.6, and 6.6 ppm revealed the presence of vinyl group.

The second step was the modification of hydrophilic clay to become organophilic to promote the compatibility with **PU**-prepolymer and hence improve the clay–matrix interactions. This step was achieved through ion exchange process between sodium cations of MMT and ammonium salt (**II**) to give organoclay ($\mathbf{I_c}$). The calcination measurements indicate that the organoclay ($\mathbf{I_c}$) contains 49.24 wt. % organic matters suggesting the presence of excess of adsorbed ammonium salt that can't be removed by washing. The third step was the synthesis of PU prepolymer **VI** by addition of an excess of **TDI** to the **PEG-1000**. The prepolymer **VI** was endcapped with **HEMA** to give acrylate terminated PU prepolymer **(VII)**.

The swelling data shown in **Tables 1, 2** indicate that the swelling degree in polar solvents such as water and acetone is very small and there is no swelling in nonpolar solvent such as benzene. It was found that the swelling behavior is increased in the polar solvents such as water and acetone than the nonpolar solvent such as benzene (the swelling followed the order water ≈ acetone > benzene). Also, the data show a small increase in the water uptake with increasing the ratio of clay which can be attributed to the higher hydrophilic characters of clay. These data reflect that there is an improvement in the solvent resistance (i.e. less permeability) of the produced materials.

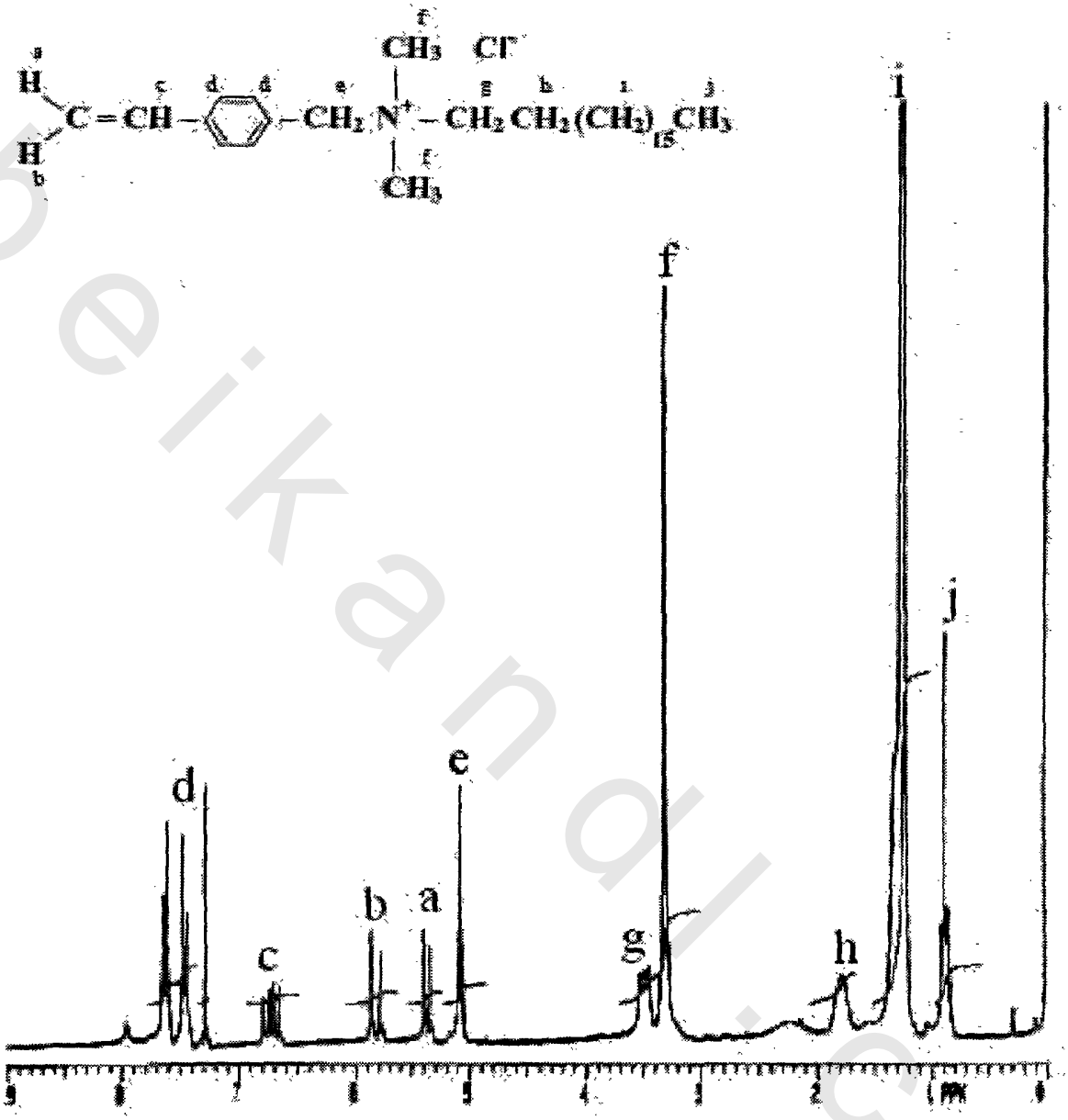

Chemical Shifts (ppm)										
Compound	H^a	H^b	H^c	H^d	H^e	H^f	H^g	H^h	H^i	H^j
VODAC	5.40	5.85	6.70	7.50	5.10	3.30	3.50	1.80	1.30	0.90

(s, 2H), 3.6(s, 6H), 1.5-0.89 (m^1H NMR ($CDCl_3$): 7.66-7.17 (m, 4H), 6.3 (dd, 1H), 5.8 (d, 1H), 5.5(d, 1H), 4.2, 37 H).

Figure 6: NMR spectra of **II**

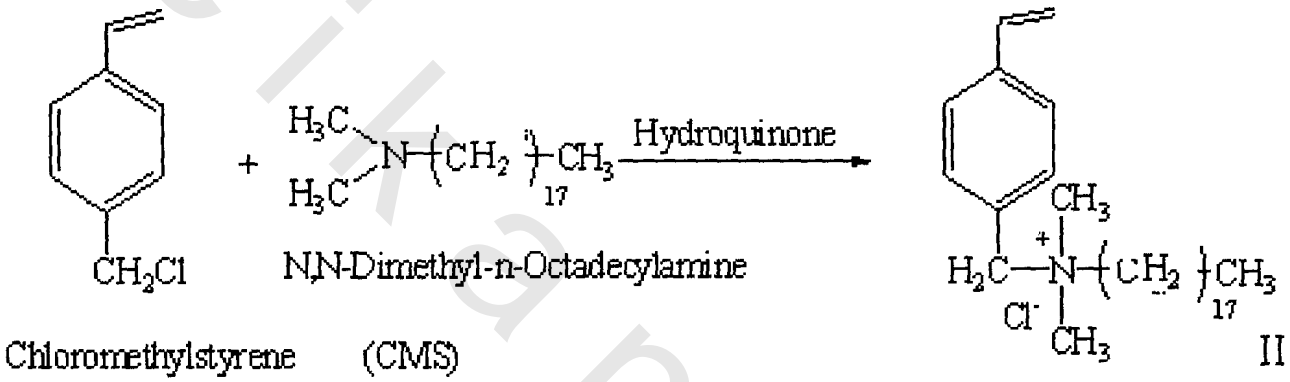

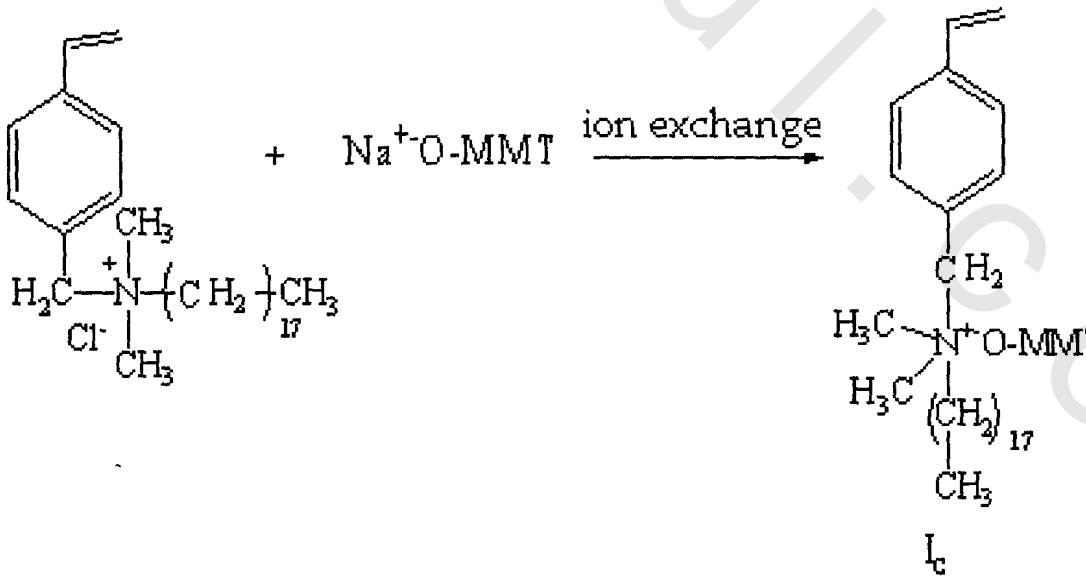

Scheme 5: Preparation of vinyl monomer-MMT

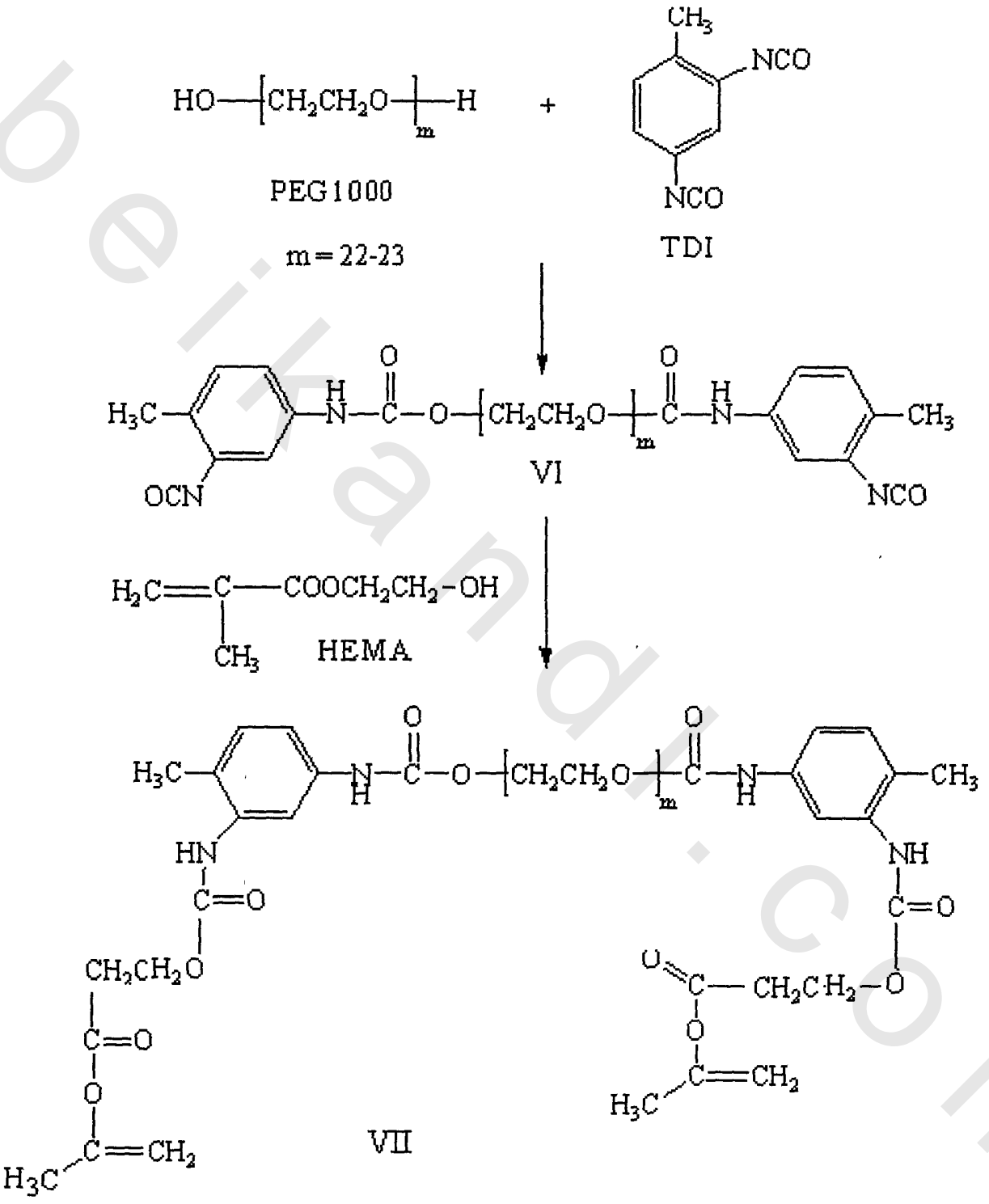

Scheme 6: Preparation of acrylate terminated **PU** prepolymer **(VII)**

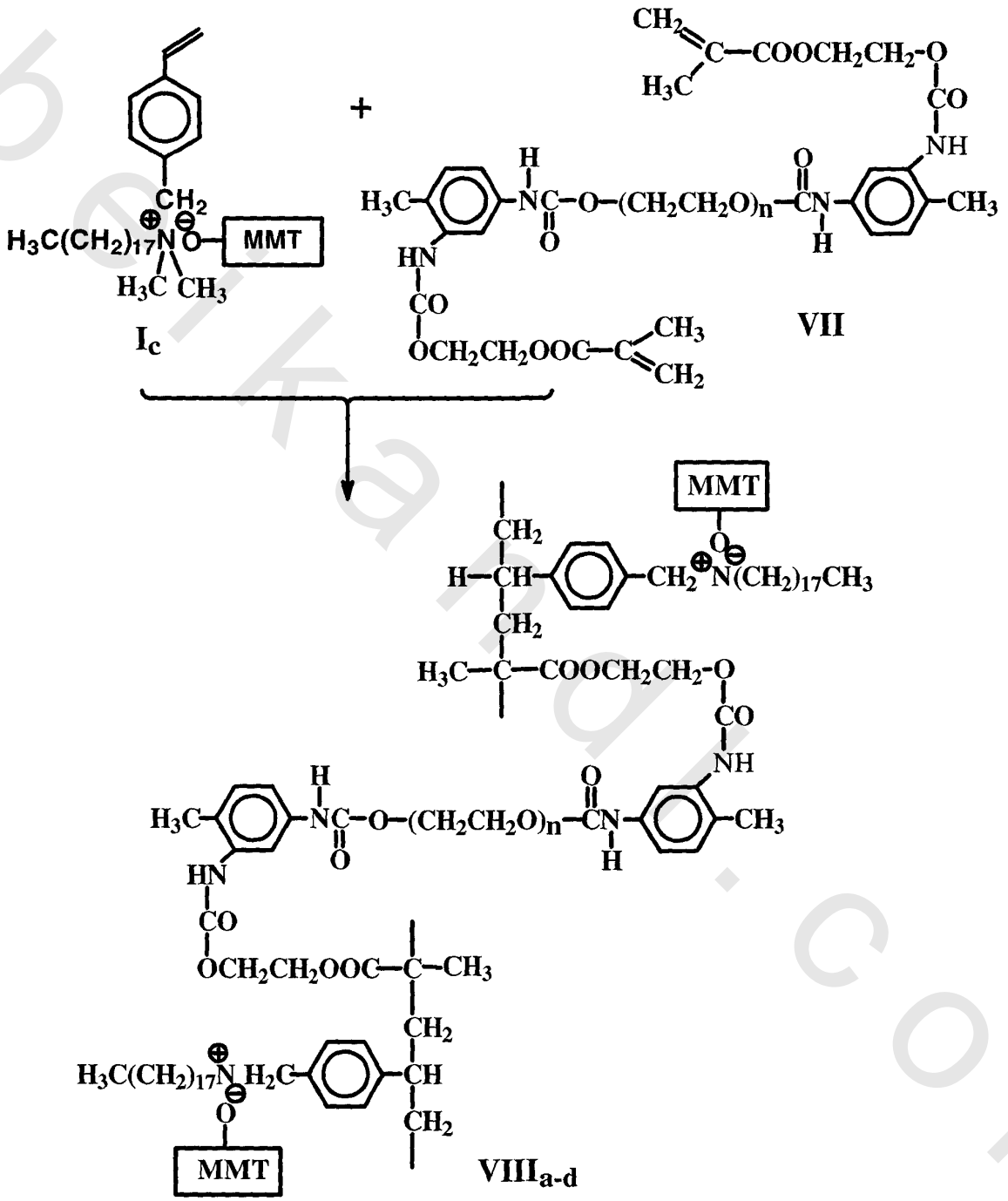

Scheme 7: Schematic diagram illustrates the synthesis of PU-organoclay nanocomposites

2. IR Spectra

IR spectra were performed to monitor the disappearance of the characteristic absorption peaks of the monomers. IR spectra of the hybrids are illustrated in **Figures 7-9**. The spectra showed that the **NH** stretching band near 3400 cm^{-1} for $\mathbf{I}_a$ and at 3430 cm^{-1} for $\boldsymbol{I}_b$, NH bending band near 1645 cm^{-1} for $\mathbf{I}_a$, and band at 1631 cm^{-1} for $\mathbf{I}_b$ are shifted quite substantially to regions associated with $^{+}NH_3$ vibration suggesting the modification of clay with ammonium salt.

A characteristic bands appear at 1039, 523, & 462 cm^{-1} for **Si-O**, at 3629 cm^{-1} for phenolic **OH** group in $\mathbf{I}_a$, at 2928,& 2852 cm^{-1} for **CH** aliphatic, and at 3608 cm^{-1} for acidic **OH** group in $\mathbf{I}_b$. The quaternary ammonium group ($-N^{+}\equiv$) show a characteristic band at 1518 cm^{-1} for $\mathbf{I}_a$ and at 1499 cm^{-1} for $\mathbf{I}_b$. The spectra show that the $^{+}NH_3$ band at 1630 cm^{-1} in organoclay is shifted to higher wavelength near 1700 cm^{-1} in nanocomposite indicating that an interaction between organoclay and the polymer was occurred.

The spectra of polyurethanes $\mathbf{III}_a$, $\mathbf{V}_a$ and $\mathbf{VIII}_a$ (**Figures 7-9**) show the absorption at 1729 cm^{-1} that is assigned to H-bonded urethane carbonyl (**C=O**) and at 1420 cm^{-1} to a secondary urethane amide (**C-NH**). The spectra of the clay modified PU $\mathbf{III}_{c\text{-}f}$ and $\mathbf{V}_c$ show peaks near 1720 cm^{-1} due to the stretching of urethane carbonyl group (**C=O**), and at 2920 & 2863 cm^{-1} for the asymmetric and symmetric C-H stretching vibration. The peak at 3309 cm^{-1} result from the N-H group in H-bonding is remained nearly the same as that of neat PU. These results indicate that there is no major change in the chemical structure of PU owing to the presence of organoclay.

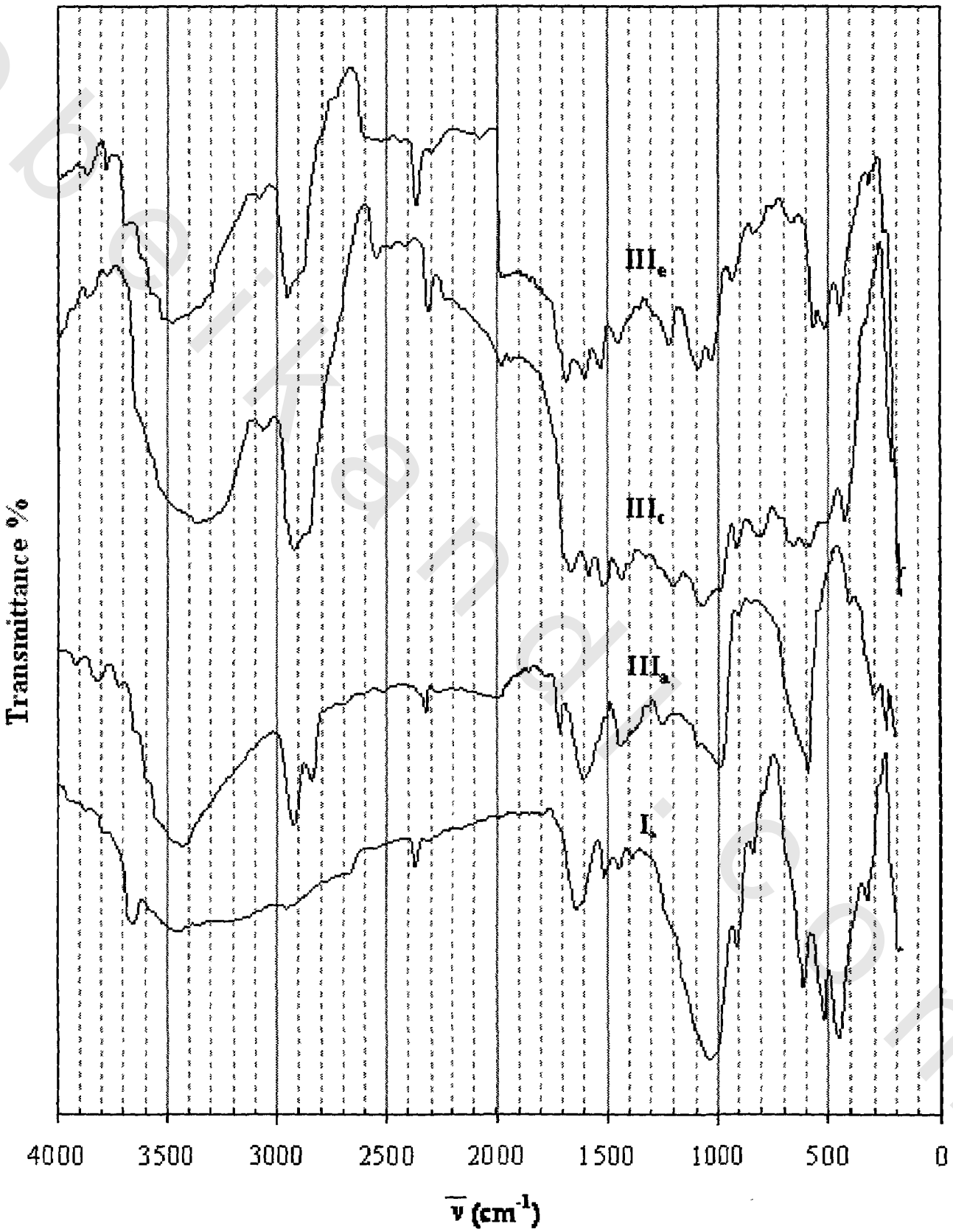

Figure 7: IR spectra for organoclay Ia, and PU-Tyr-MMT $\mathbf{III}_{a,c,e}$

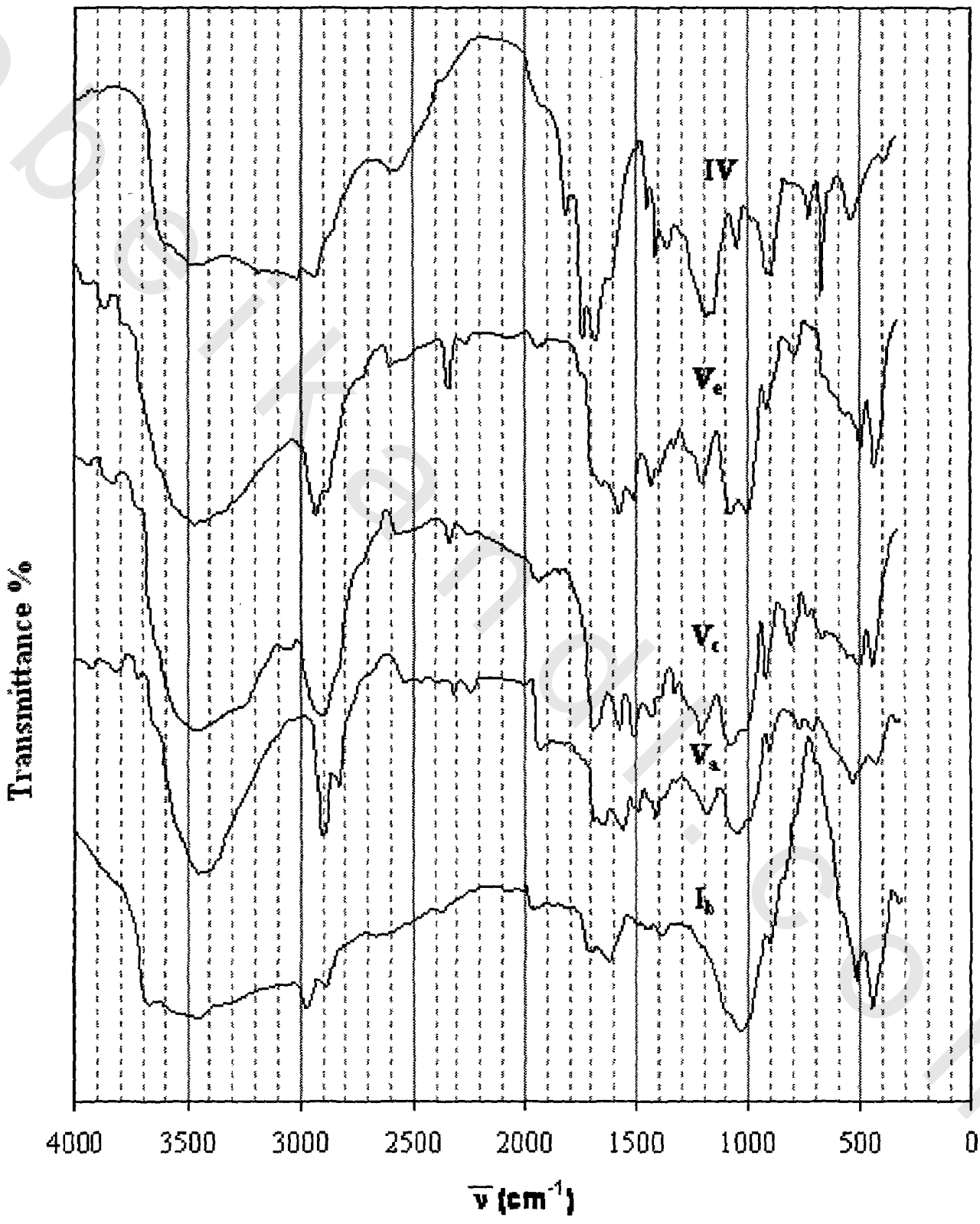

Figure 8: IR spectra for organoclay I_b, copolymer **IV** and PU-organoclay $V_{a, c, e}$

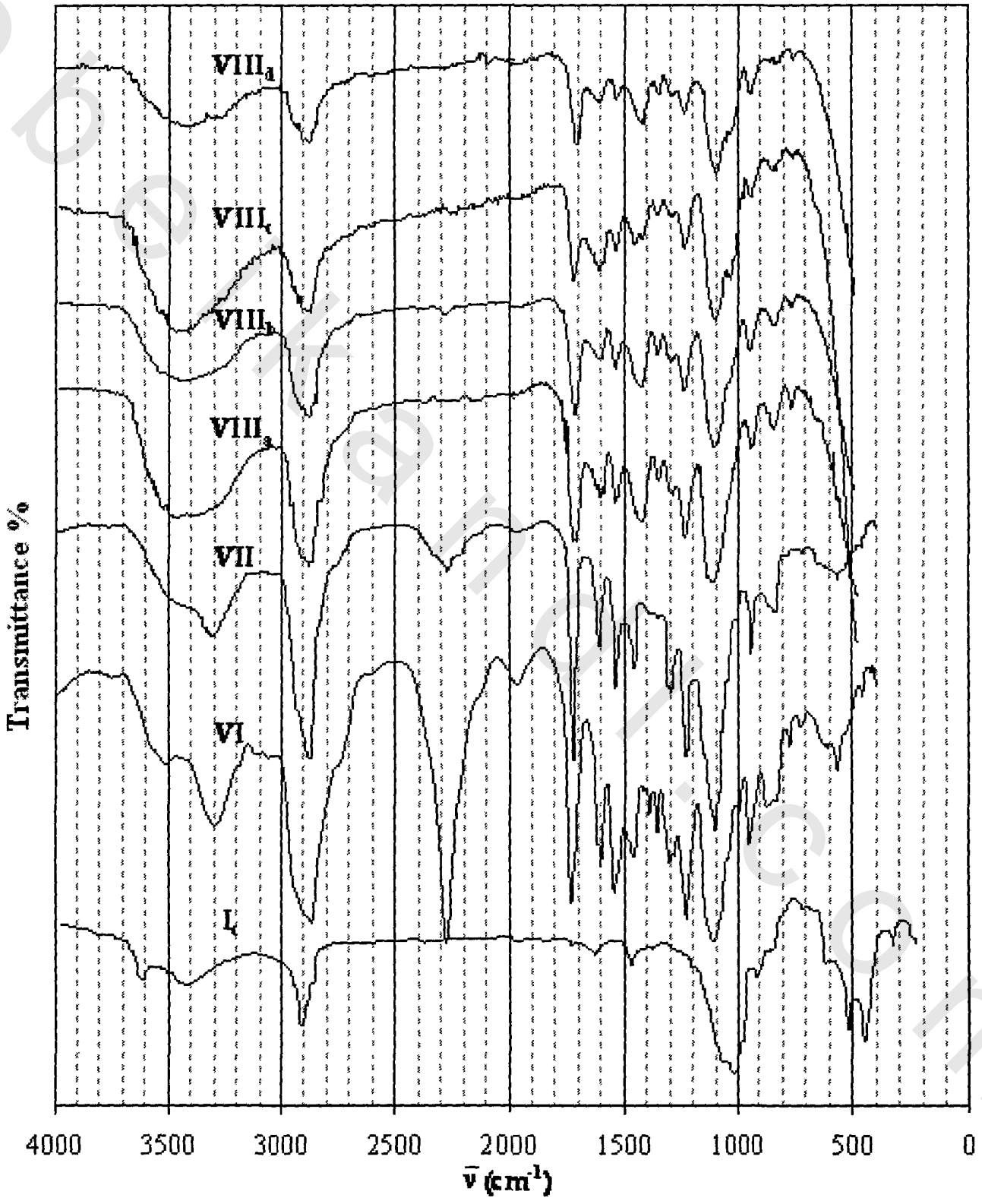

Figure 9: IR spectra of **Ic**, **VI**, **VII** and **VIII$_{a-d}$**

Figure 9 shows the **IR** spectra of vinyl monomer-MMT ($\mathbf{I_c}$), polyurethane prepolymer **VI**, acrylate-end capped PU (**VII**) and PU–organoclay hybrids (**$\mathbf{VIII_{a-d}}$**). The spectrum of $\mathbf{I_c}$ showed that the band at 838 cm^{-1} related to **C–Cl** of chloromethyl groups was disappeared. It shows also a characteristic band corresponding to the ammonium salt, $\mathbf{N^{\oplus}(R)_3}$, at 3433 cm^{1} is present. An intense strong band at 2260 cm^{-1} characteristic for the isocyanate group of PU prepolymer (end capped with free isocyanate) which appears as a weak band in PU endcapped with vinyl group indicates traces of isocyanate still present that completely disappeared after curing in PU nancomposites. It shows characteristic bands at 1629 cm^{-1} related to vinyl group for **Ic,** at 1603 cm^{-1} for vinyl group of **HEMA**, and at 750 cm^{-1} characteristic for CH_2 of **PHEMA** (**VIIIa-d**) [137].

3. Thermal Analysis

Thermal analysis of polyurethane-clay materials were determined by both calcination at 1000 °C and **TGA** under both argon and air atmosphere. The **TGA** thermograms of the samples **$\mathbf{III_{a-f}}$**, **$\mathbf{Va_{-e}}$** and **$\mathbf{VIII_{a-d}}$** are shown in **Figures 10-14** and the data are summarized in **Tables 1-4**. The weight loss encountered during heating of PU-organoclay hybrids are found in the range of 84 -97 % as determined by both **TGA** under air atm. and calcination (**Tables 1-3**). The **TGA** curves for the samples **$\mathbf{III_{a-f}}$** and **$\mathbf{V_{a-e}}$** are shown in **Figures 10-13** indicate that there are two stages of decomposition. The first stage is sharp and major, which involves the thermal decomposition of the organic part of the hybrid. The decomposition temperatures in this stage are in the range of ~ 250 - 400 °C, corresponding to weight loss ranging from 65% to 80%. In this stage, the difference between the samples is very small

without any order can be mentioned. The second stage is broad, in which the weight loss is ranged from 17% to 22% in the temperature range at ca.400°C to ca.570°C. In this stage, the composites display higher thermal resistance than neat polymers. This stage is attributed to further decomposition of the rest of intercalated polymer, especially the intercalated polymer into the interlayer spacing of the clay, the intercalating agent of clay, and the loss of **OH** groups and the crystallographic structure collapsed [138]. Generally, the hybrids are degraded at nearly the same temperature range and slightly faster than pure PU in the first stage. However, in the second stage, after complete decomposition of the small organic molecules, all the nanocomposites show higher thermal resistance than neat PU matrices [139]. **TGA** of the samples $III_{a\text{-}f}$ and $V_{a\text{-}e}$ was also studied under argon atmosphere to avoid the oxidative degradation effect of air atmosphere.

It was found that there are differences in the **TGA** under argon than in air. This was explained for two reasons: the first is the presence of oxygen in air which helps in increasing rates of decomposition. The second is due to the higher thermal conductivity of air than argon, which leads to slower decomposition rates under argon than in air [140] as illustrated in **Tables 3& 4** and **Figures 11** & **13**. The data in the Tables **3** & **4** show that the temperature at which the samples lose 5% and 10% of its weight is higher under argon than in air for all the samples. **TGA** thermographs analysis under argon for the samples $\mathbf{III_c}$ and $\mathbf{III_d}$ indicated that the maximum rates of pyrolysis are 21.15 and 20.38% per minute at 426°C and 418°C respectively as shown in **Figure 15**. These results indicate that the thermal properties are improved with increasing the content of clay up to 10 wt. % loading as illustrated in **Figures 11 & 13**. Thermal properties of clay modified PU materials ($\mathbf{III_{a\text{-}f}}$, $\mathbf{V_{a\text{-}d}}$) were investigated by both calcinations and **TGA** under

argon. The data are summarized in **Table 5**. **Figure 14** shows that the weight loss encountered during heating the PU–organoclay hybrids (**VIII$_{a-d}$**) are found in the range from 75- 87% as determined by TGA. The calcination measurements show a correlation between the theoretical calculations and experimental results of the clay contents.

The TGA under nitrogen atmosphere for the samples **VIII$_{a-d}$** shown in **Figure 14** indicates that there is a small difference in thermal resistance of samples at temperature in the range 260 °C to 326 °C, which involves the thermal decomposition of the organic materials (modifier) present on the surface of the layers of the clay. In the temperature range 280 °C to 503 °C the composites display higher thermal resistance than neat polymer. This is attributed to further decomposition of the rest intercalated polymer.

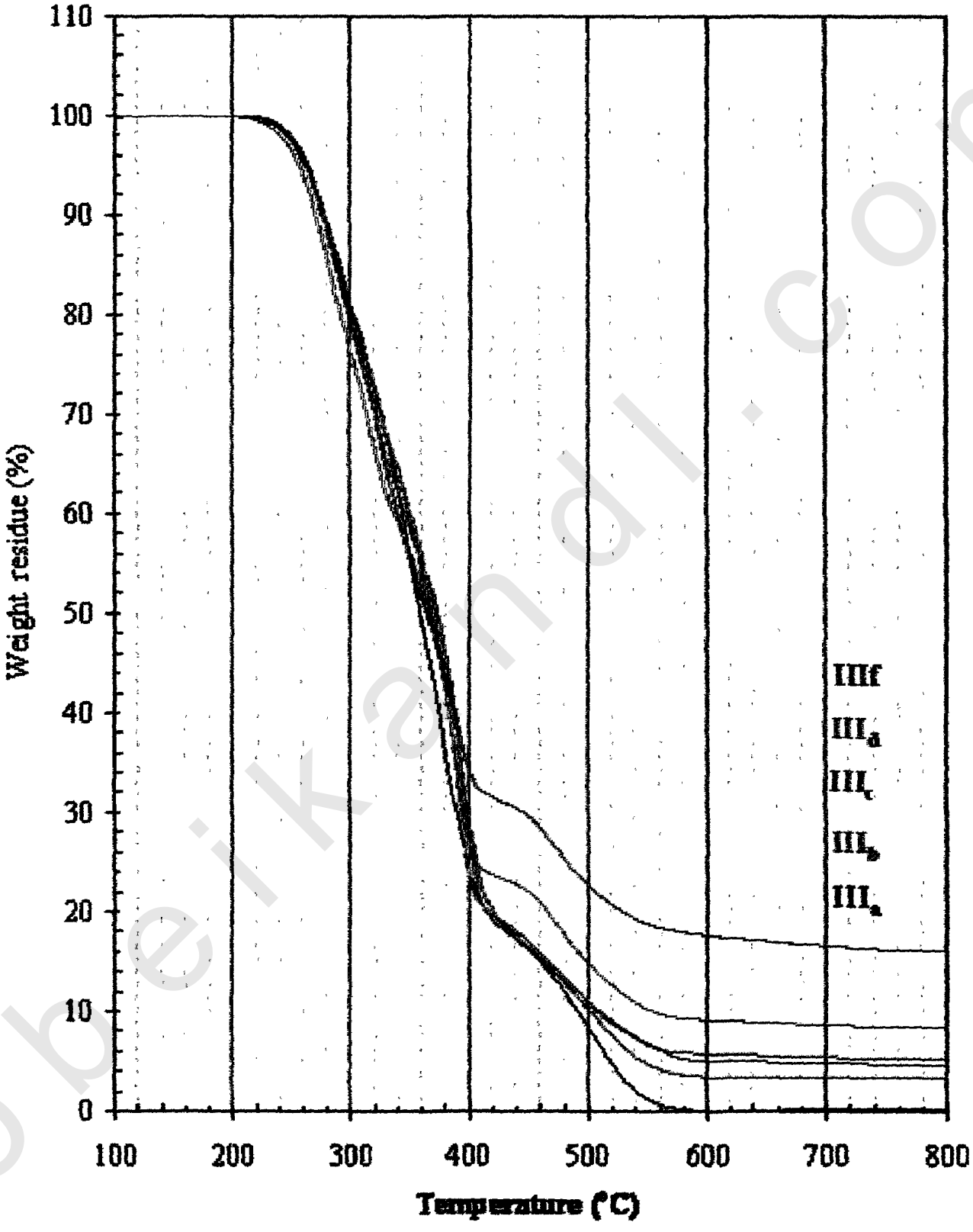

Figure 10: TGA thermographs for PU/ Tyr-MMT nanocomposites (III_{a-f}) in atmospheric air

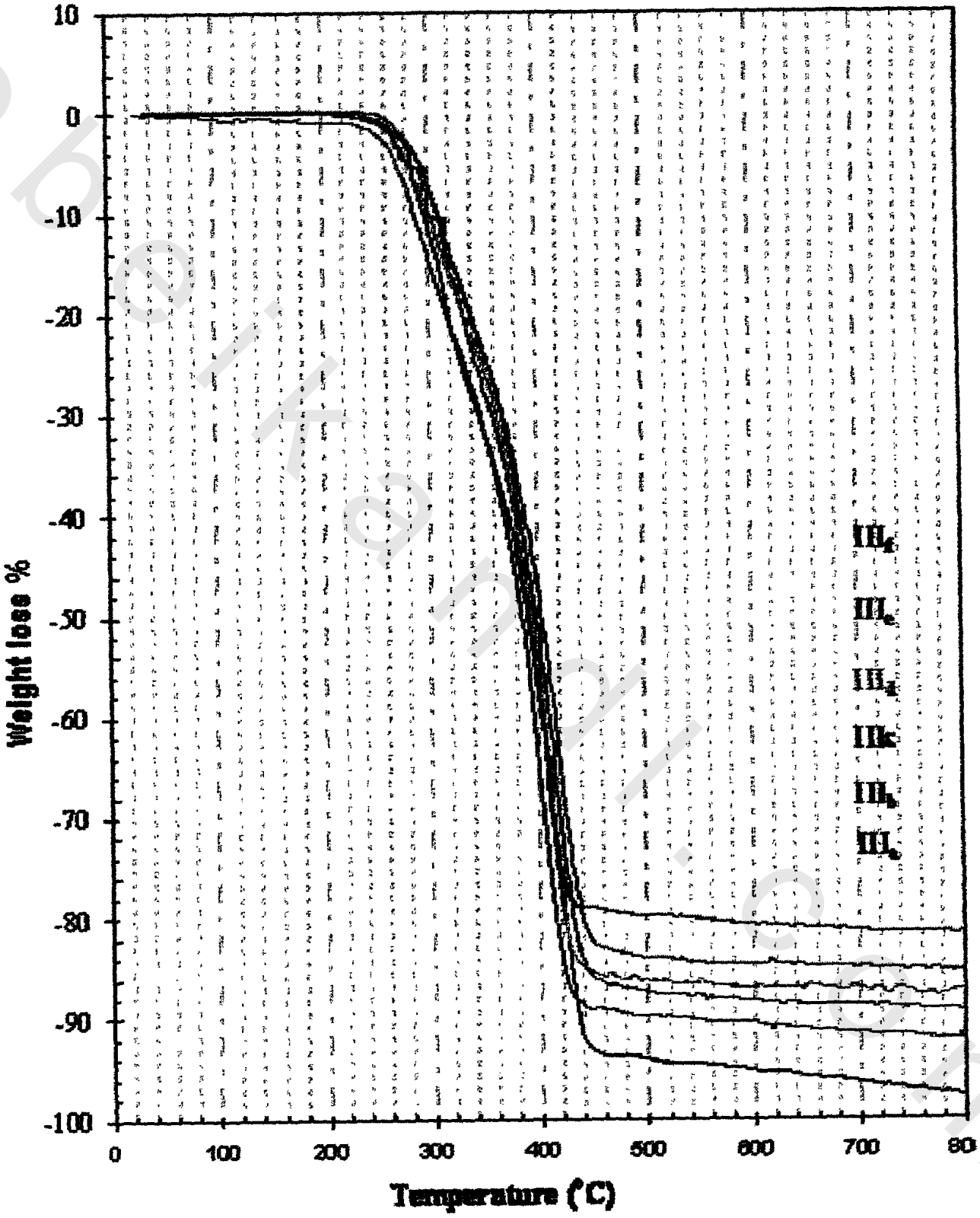

Figure 11: TGA thermographs under argon atmosphere for **PU**-organoclay composites **III$_{a-f}$**. (Tyr-MMT)

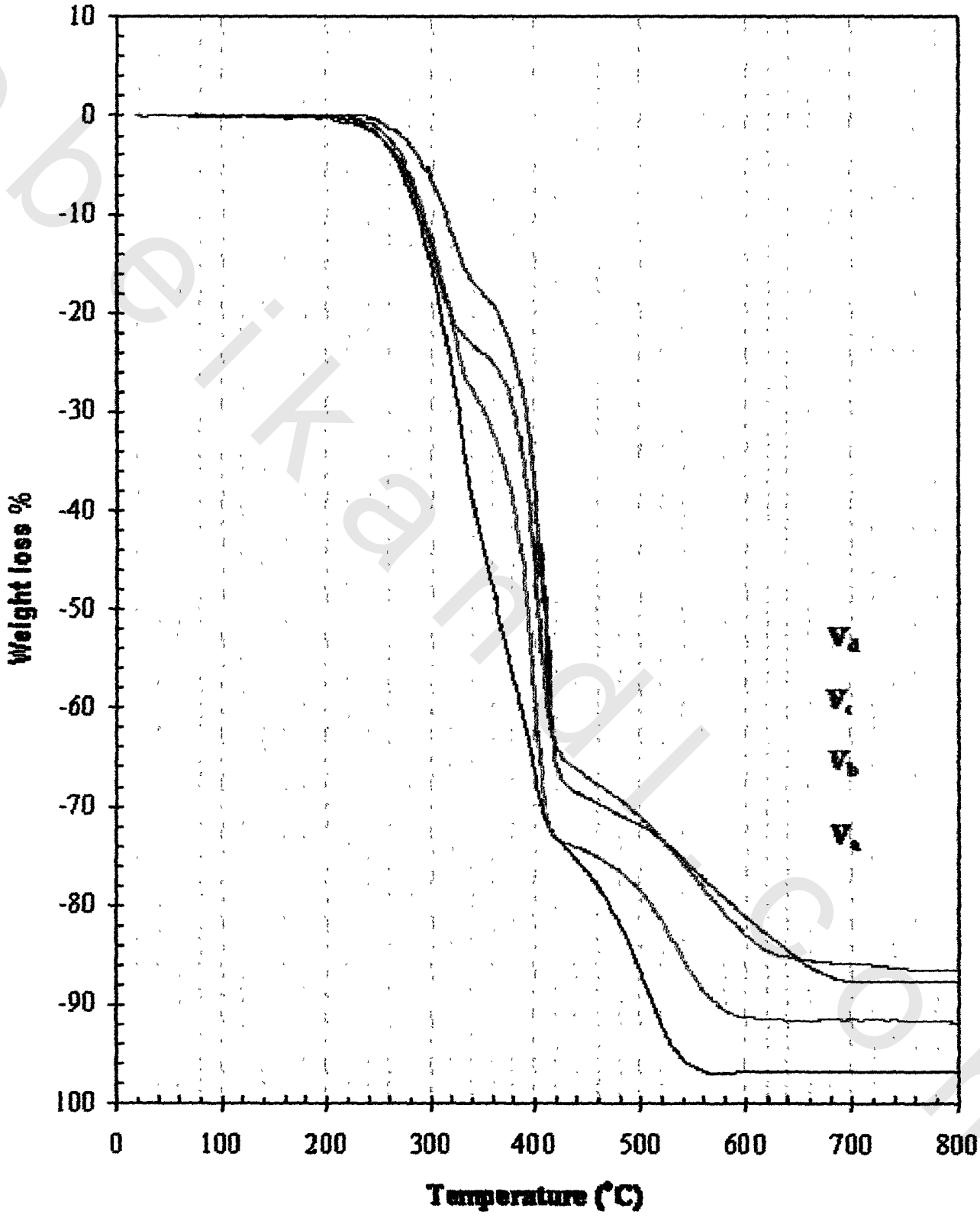

Figure 12: TGA thermographs for the PU-organoclay samples V_{a-d} in atmospheric air

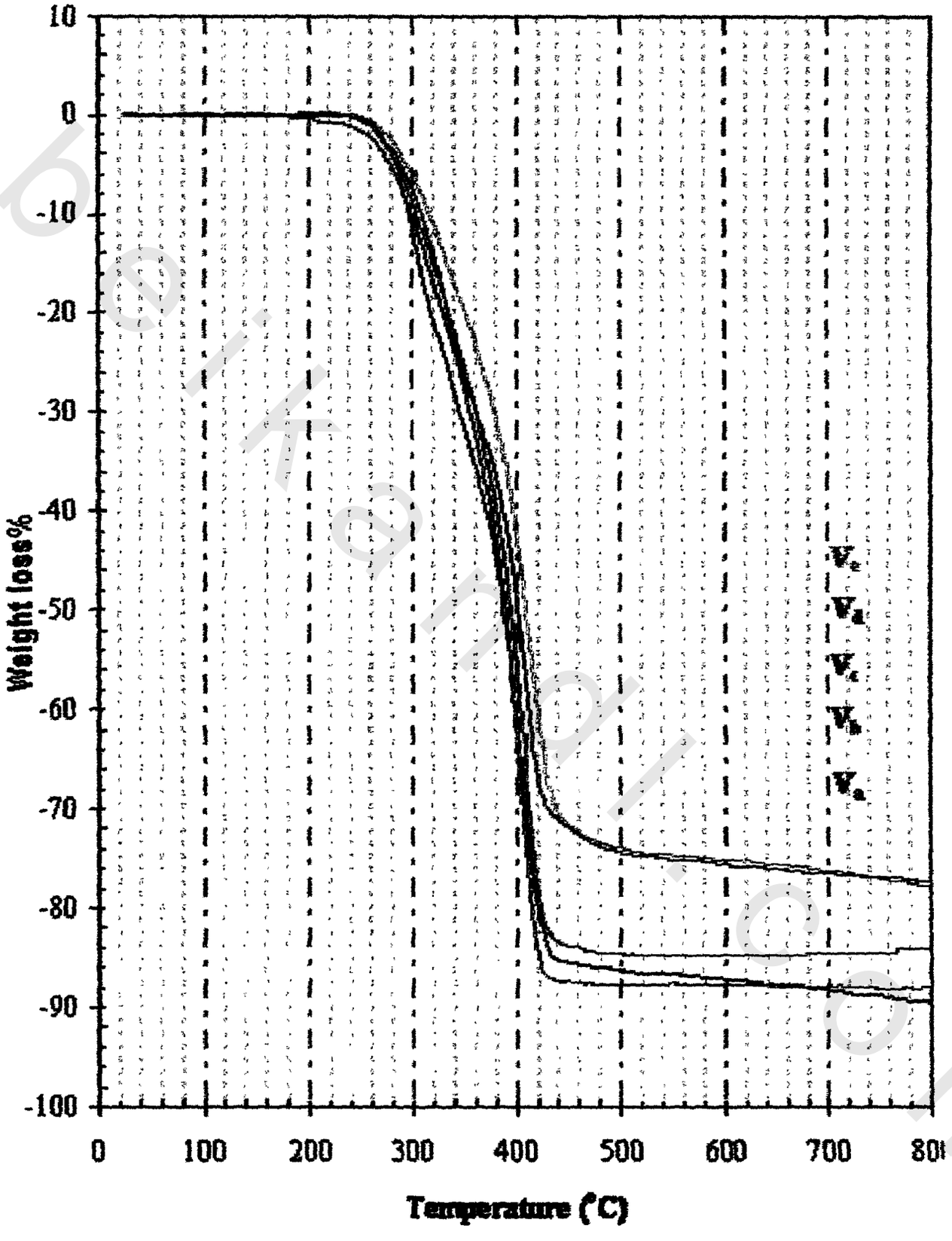

Figure 13: TGA thermographs for the PU-organoclay samples V_{a-e} under argon atmosphere

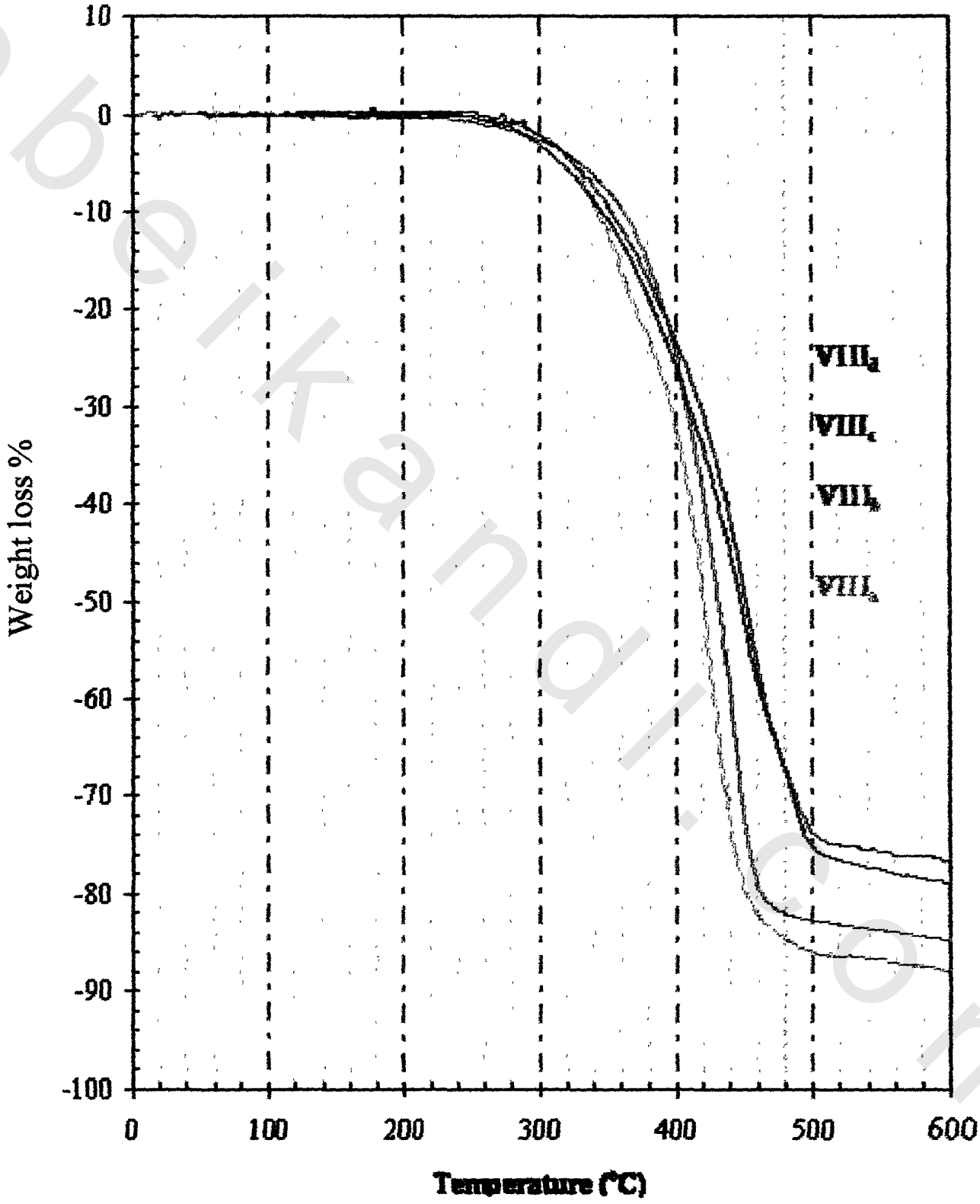

Figure 14: TGA Thermographs of **VIII$_{a-d}$** under nitrogen atmosphere

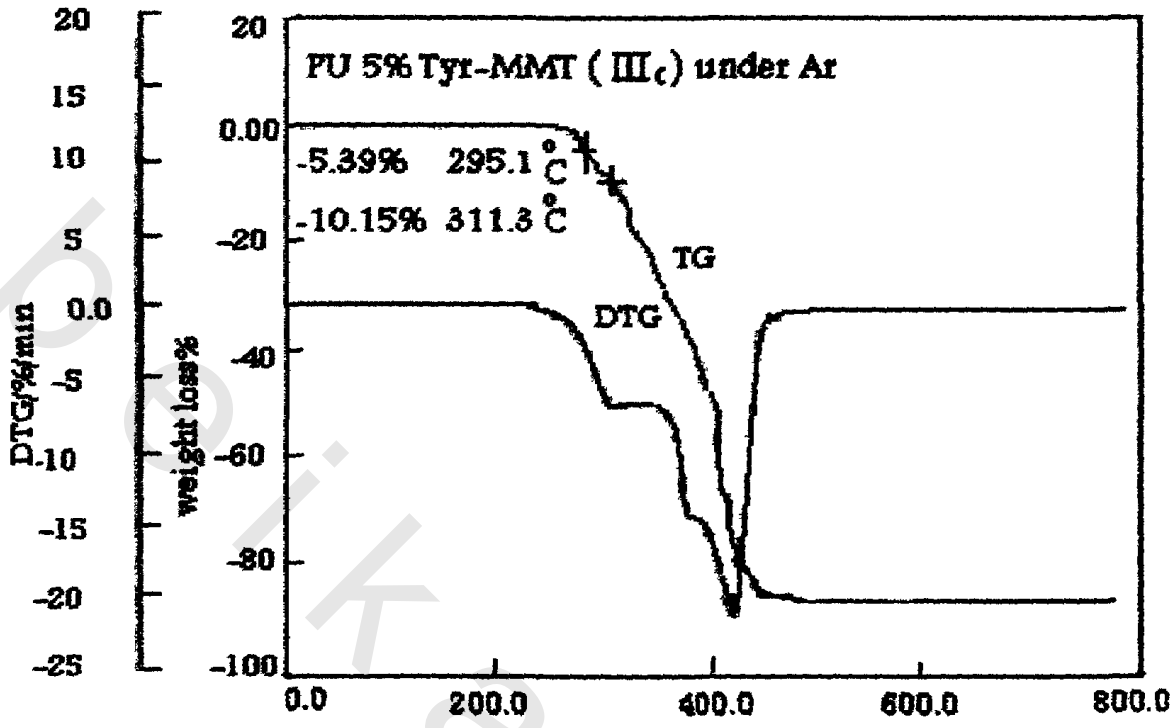

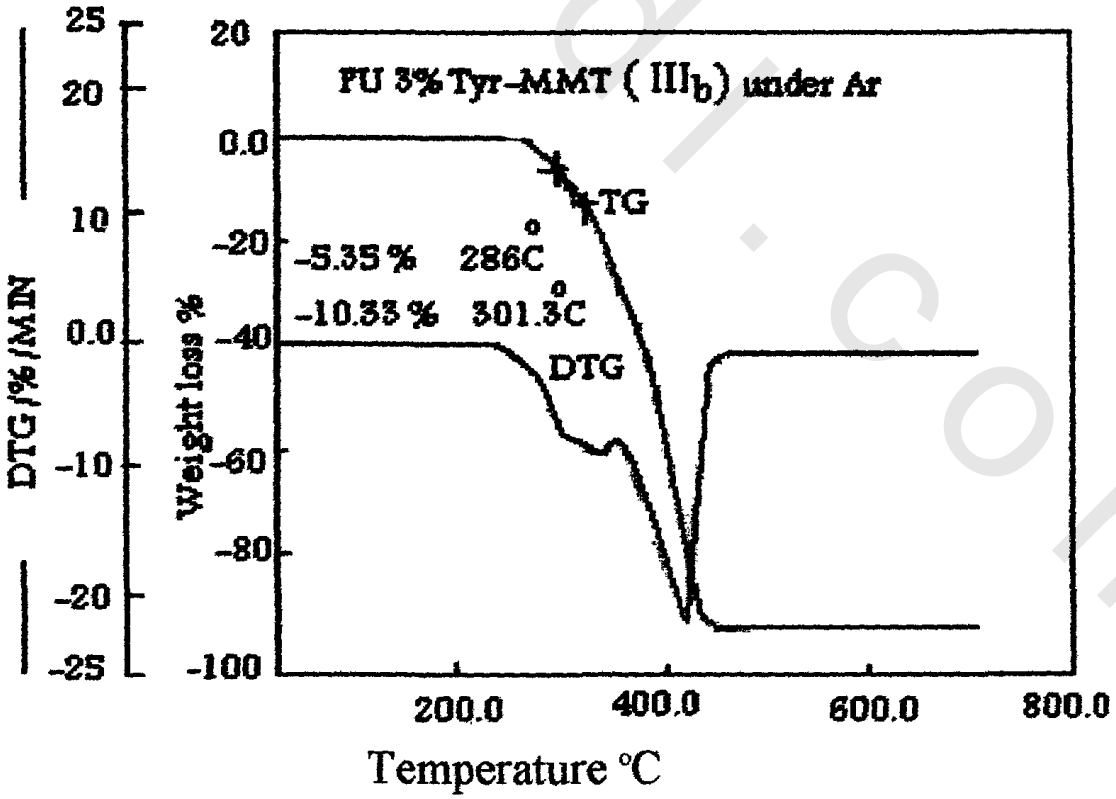

Figure 15: TGA and DTG of III_b and III_C

Table 1: Swelling, calcinations and char yield data of PU-Tyr-MMT nanocomposites $\mathbf{III_{a-f}}$

Sampe	$\mathbf{I_a}$	Swelling [1]			Calcination[2]					Char Yield (%)[3]	
	Wt-%	Water (%)	Acetone (%)	Benzene (%)	dry Weight (g)	Residue (g)	Weight loss (g)	Clay (%)	Organic contents (%)	In Air	In Argon
$\mathbf{III_a}$	00	0.98	0.58	0.13	0.9324	0.0000	0.9324	0.00	100	0.00	7.90
$\mathbf{III_b}$	3	0.84	0.57	0.10	0.8781	0.0230	0.8551	2.62	97.38	3.22	----
$\mathbf{III_c}$	5	0.76	0.48	Nil	0.9405	0.0411	0.8994	4.37	95.63	4.62	10.92
$\mathbf{III_d}$	7	0.79	0.43	Nil	0.9311	0.0492	0.8819	5.28	94.72	5.32	12.45
$\mathbf{III_e}$	10	1.58	0.26	Nil	0.7881	0.0658	0.7223	8.35	91.65	8.42	13.16
$\mathbf{III_f}$	20	1.67	0.22	Nil	0.7931	0.1270	0.6661	16.01	83.99	16.04	17..97

[1] Calculated by [adsorbed solvent (g) x 100/dry sample (g)].

[2] At 1000 °C for 8h

[3] At 900°C

Table 2: Swelling, calcinations and char yield data of PU-SMA/ALA-MMT nanocomposites $\mathbf{V_{a-e}}$

Sample	Organoclay	Swelling [1]			Calcination[2]					Char Yield (%)[3]	
	$\mathbf{I_b}$ (Wt-%)	Water (%)	Acetone (%)	Benzene (%)	dry Weight (g)	Residue (g)	Weight loss (g)	Clay (%)	Organic contents (%)	In Air	In Argon
$\mathbf{V_a}$	00	0.93	0.67	0.15	0.9271	0.0000	0.9271	0.00	100.00	3.21	9.10
$\mathbf{V_b}$	1	0.71	0.62	Nil	0.8834	0.0067	0.8767	0.76	99.24	-----	13.09
$\mathbf{V_c}$	5	1.25	0.57	Nil	0.8562	0.0325	0.8237	3.80	96.20	8.40	15.55
$\mathbf{V_d}$	10	1.46	0.5	Nil	0.7921	0.0578	0.7343	7.30	92.70	11.37	21.75
$\mathbf{V_e}$	20	1.68	0.24	Nil	0.8356	0.1154	0.7202	13.81	86.19	13.95	22.25

[1] Calculated by [adsorbed solvent (g) x 100/dry sample (g)].

[2] At 1000°C for 8h.

[3] At 900°C

Table 3: Thermal analysis data of PU-Tyr-MMT nanocomposites (**III_{a-f}**)

Sample	I_a	TGA Data												Calcination	
		Under air									Under argon			Clay	Organic
		Tem. at	Tem. at	1 st step			2 nd step			Char yield	Tem. at	Tem. at	Char yield	contents	contents
	(%)	d-5%	d-10%	Start	End	%-Wt loss	Start	End	%-Wt loss	(%)	d-5%	d-10%	(%)	(%)	(%)
III_a	00	----	----	---	---	---	---	----	---	0.00	271	287	7.90	0.00	100
III_b	3	265	279	246	448	82,	449	588	98	3.38	286	301	3.22	2.62	97.38
III_c	5	262	278	255	423	81	424	583	96	4.64	295	311	10.92	4.37	95.63
III_d	7	264	277	244	419	83	245	603	94.5	5.32	283	300	12.45	5.28	94.72
III_e	10	275	272	326	427	80	327	606	93.3	8.42	297	314	13.16	8.35	91.65
III_f	20	264	279	---	---	---	---	---	---	16.04	280	293	17.97	16.01	83.99

Table 4: Thermal analysis data of PU-SMA-ALA-MMT nanocomposites (V_{a-e})

Sample	I_b	TGA Data												Calcination	
		Under air									Under argon			Clay	Organ
		Temp. at	Temp. at	1 st step			2 nd step			Char yield	Temp at	Temp at	Char yield		conte
	(%)	d-5%	d-10%	Start	End	%-Wt loss	Start	End	%-Wt loss		d-5%	d-10%	(%)	(%)	(%)
V_a	00	268	286	262	344	39.82	345	415	72.78	3.21	286	298	9.10	0.00	100.0
V_b	1	---	---	---	---	----	---	---	---	-----	294	311	13.09	0.76	99.2
V_c	5	271	290	241	339	28.23	340	420	73.74	8.40	290	309	15.55	3.80	96.2
V_d	10	292	312	282	346	18.18	347	435	69.33	11.37	296	315	21.75	7.30	92.7
V_e	20	268	287	267	336	23.26	337	425	65.02	13.95	280	300	22.25	13.81	86.1

Table 5: Thermal stability of PU-Organoclay Hybrids **$VIII_{a-d}$**

Sample	I_c (%)	TGA Data							Calcination measurements	
		Temp. at	Temp. at	Temp. At	DTG			Char Yield	Organic Contents	Inorganic Contents
		d-5%	d-10%	d-50%	Start Temp.	End Temp	%-Wt Loss	(%)	(%)	(%)
$VIII_a$	0	326	344	420	287-371	370-469	20-83	13	100	0
$VIII_b$	3	331	362	430	318	473	81	16	98.46	1.54
$VIII_c$	7	327	354	452	308	502	83	22	96.4	3.6
$VIII_d$	10	317	346	448	305	503	75	25	94.9	5.1

4. Mechanical Behaviors

The mechanical properties of PU-organoclay nanocomposites were investigated by measuring the tensile strength and elongation. The data are illustrated in **Tables 6-8** and **Figures 16-23.** The data in the **Tables 6, 7** and **Figures 16, 17** shows that the tensile strength values of $\mathbf{III_{a-f}}$ and $\mathbf{V_{a-e}}$ are increased with increasing the organoclay contents at pK_{max}. The tensile strength values of $\mathbf{III_a}$ and $\mathbf{V_a}$, containing zero percent organoclay content are found 114 and 787 Kg/cm^2 at pK_{max}, which are increased to 195, 1111 at 5%-wt organoclay; 215, 1223 at 10%-wt organoclay; and 221, 1427 Kg/cm^2 at 20%-wt organoclay. **Figures 16&17**, illustrate that the tensile strength is highly affected by the clay contents especially with the small ratios of clay. The figures show that the increasing rates of tensile strength at pK_{max} are larger with small contents (1–5%-wt) of organoclay than with the high organoclay contents. This can be attributed to increasing the hardness of the films due to the presence of rigid clay layers. Also, the tensile strength at break is increased with the same manner as at pK_{max} with the small quantity of organoclay (3%) followed by gradual decrease with increasing the organoclay content.

The tensile strength values of the third series $\mathbf{VIII_{a-d}}$ illustrated in **Table 8** and **Figure 18** show that the sample $\mathbf{VIII_a}$ containing 0% of organoclay found 80.2 kg/cm^2 at pk_{max}, which is increased to 146.1, 169.8 & 177.3 kg/cm^2 with organoclay content 3%, 7%, 10%, respectively. The data show that the tensile strength values affected by the clay contents especially with the small ratios. Also, the tensile strength at break is increased with the same manner at pk_{max} with small quantity of organoclay (3%) followed by gradual decrease with increasing the organoclay ratios. This data was

corresponding to the other samples. This due to increasing the brittleness and the materials start to lose the mechanical properties after the point of pK_{max}.

The data in the **Tables 6, 7** and **Figures 19, 20** illustrate the elongation values of the samples $\mathbf{III_{a-f}}$ & $\mathbf{V_{a-e}}$ at pK_{max} and at break, which are decreased with increasing the clay contents due to increasing the film strength. It was found that the elongation nearly the same at pK_{max} and at break. The figure shows that the elongation rate is larger with small contents (1-5%) of organoclay than with the high contents (10-20%). The data in **Table 8** and **Figure 21** for the hybrids $\mathbf{VIII_{a-d}}$, illustrate that the elongation values at pk_{max} and at break are increased with increasing the organoclay contents. This can be attributed to the further extension with the n-octadecyl chain. The polymerization methods take into account the possibility of the formation of clay tethered polymeric chains via reactions between vinyl groups in the chains of polyurethane and vinyl groups on organic modifier of clay through free radical polymerization [121-123].

Figures 22, 23 and **Tables 6-8** illustrate a comparison between **PU/ Tyr-MMT** ($\mathbf{III_{a-f}}$), **PU/ SMA–ALA–MMT** ($\mathbf{V_{a-e}}$) and PU–Organoclay ($\mathbf{VIII_{a-d}}$) materials. The figures and Tables show that the tensile strengths values of $\mathbf{III_{a-f}}$ and $\mathbf{VIII_{a-d}}$ are nearly the same quantity and manner. While, the hybrids $\mathbf{V_{a-e}}$ show higher tensile strength than the hybrids $\mathbf{III_{a-f}}$ and $\mathbf{VIII_{a-d}}$ with 6–7 times. This can be attributed to the presence of **PSMA**, which gave superior mechanical properties, due to its hardness, stiffness as well as interaction with PU matrix.

It was found that the elongation values (**Figure 23**) of the samples $\mathbf{III_{a-f}}$ are higher than the values of the samples $\mathbf{V_{a-e}}$ but they are decreased in the same manner with increasing the clay contents. While the elongation values of the samples $\mathbf{VIII_{a-d}}$ are increased with increasing the clay contents, which

reflect the flexibility of the films due to ester and urethane linkages in the polymer matrix and the presence of n–octadecyl chain attached to the MMT

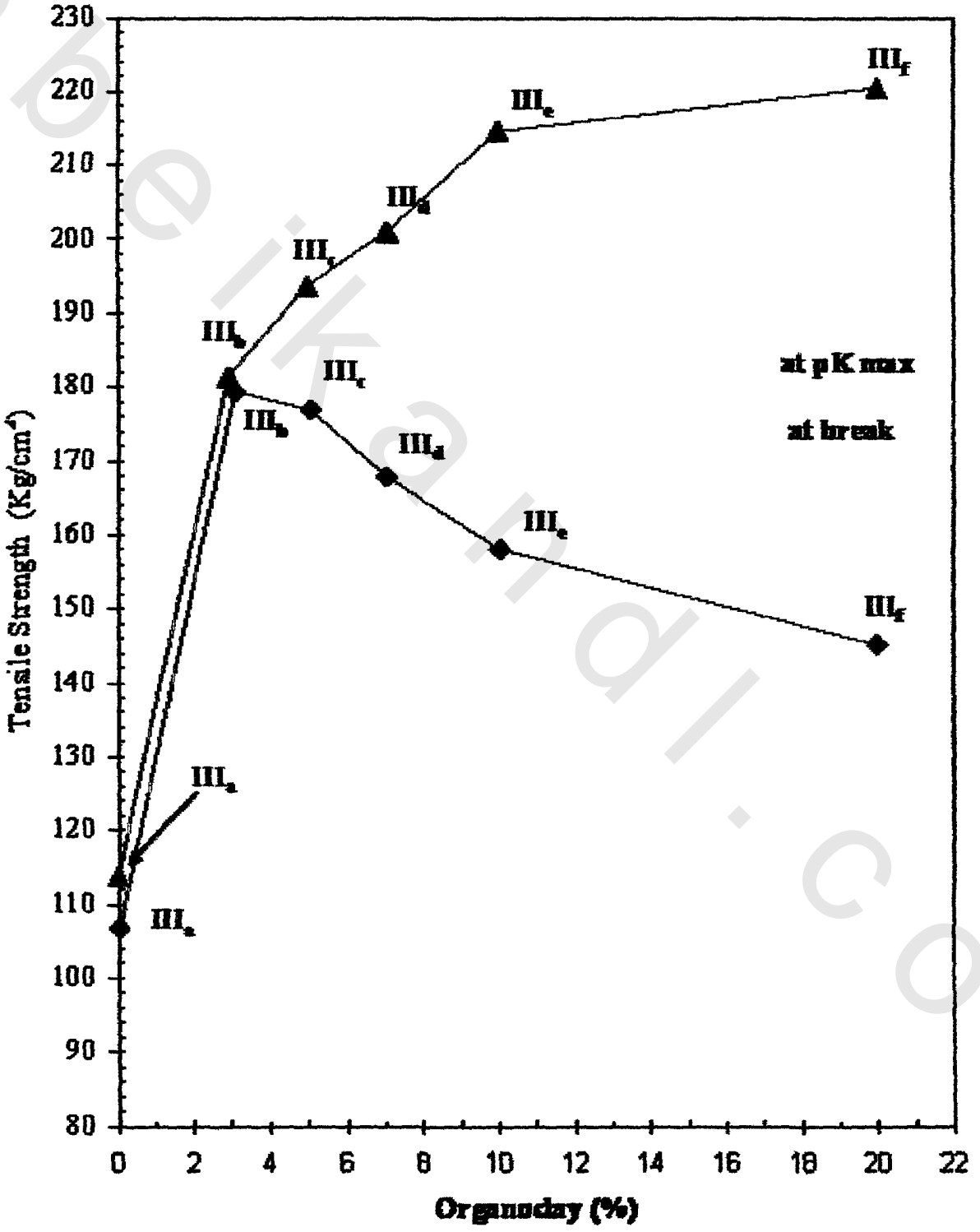

Figure 16: Tensile strength versus organoclay content for PU/Tyr-MMT nanocomposites (III_{a-f}) at pKmax and at break

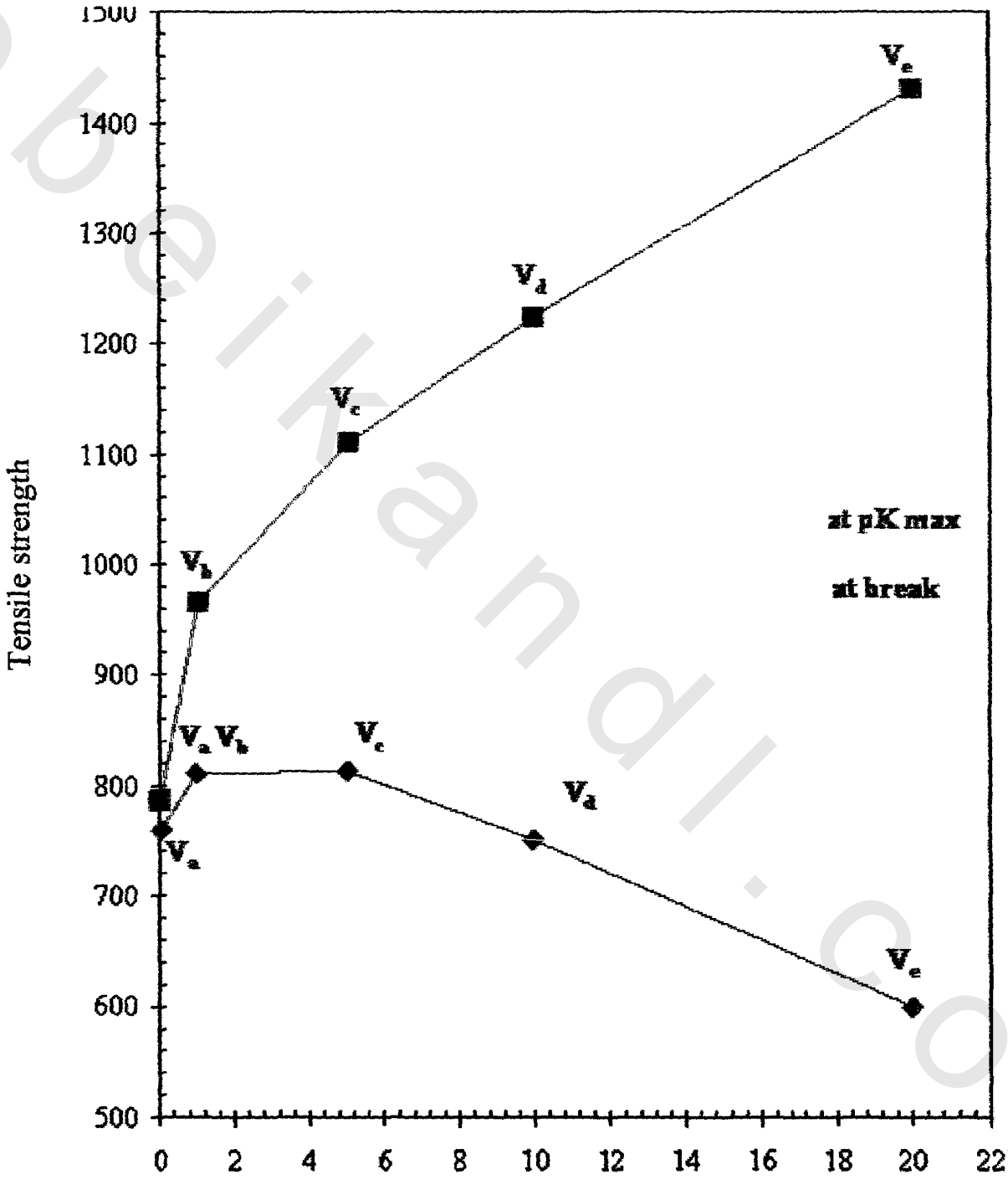

Figure 17: Tensile strength versus organoclay content for PU/SMA-ALA-MMT nanocomposites(V_{a-e})at pKmax and at break

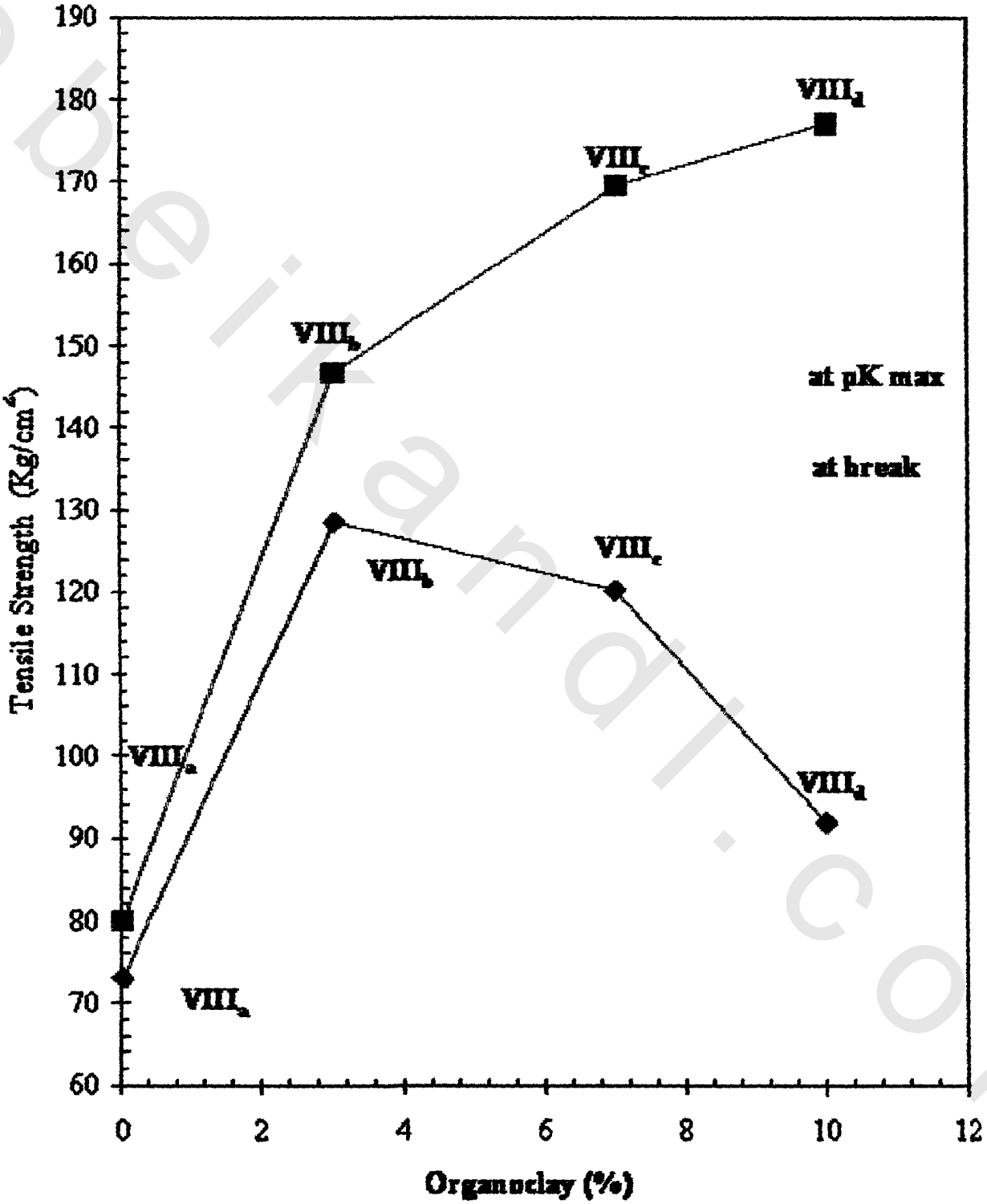

Figure 18: Tensile strength versus organoclay content for PU/ vinyl monomer-MMT nanocoposites ($VIII_{a-d}$) at pK max and at break

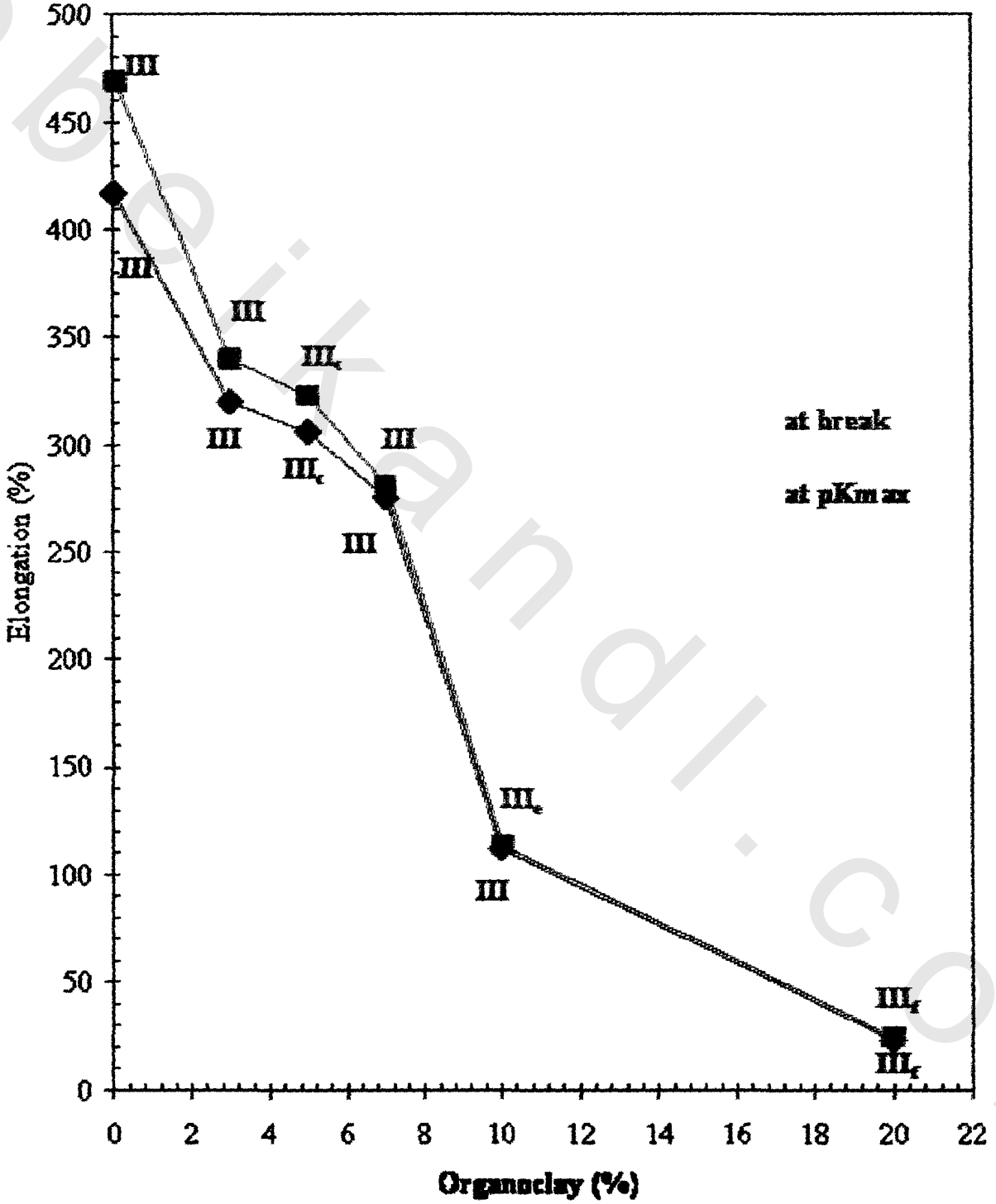

Figure 19: Elongation versus organoclay content for PU/ Tyr -MMT nanocomposites (III_{a-f}) at pK_{max} and at break

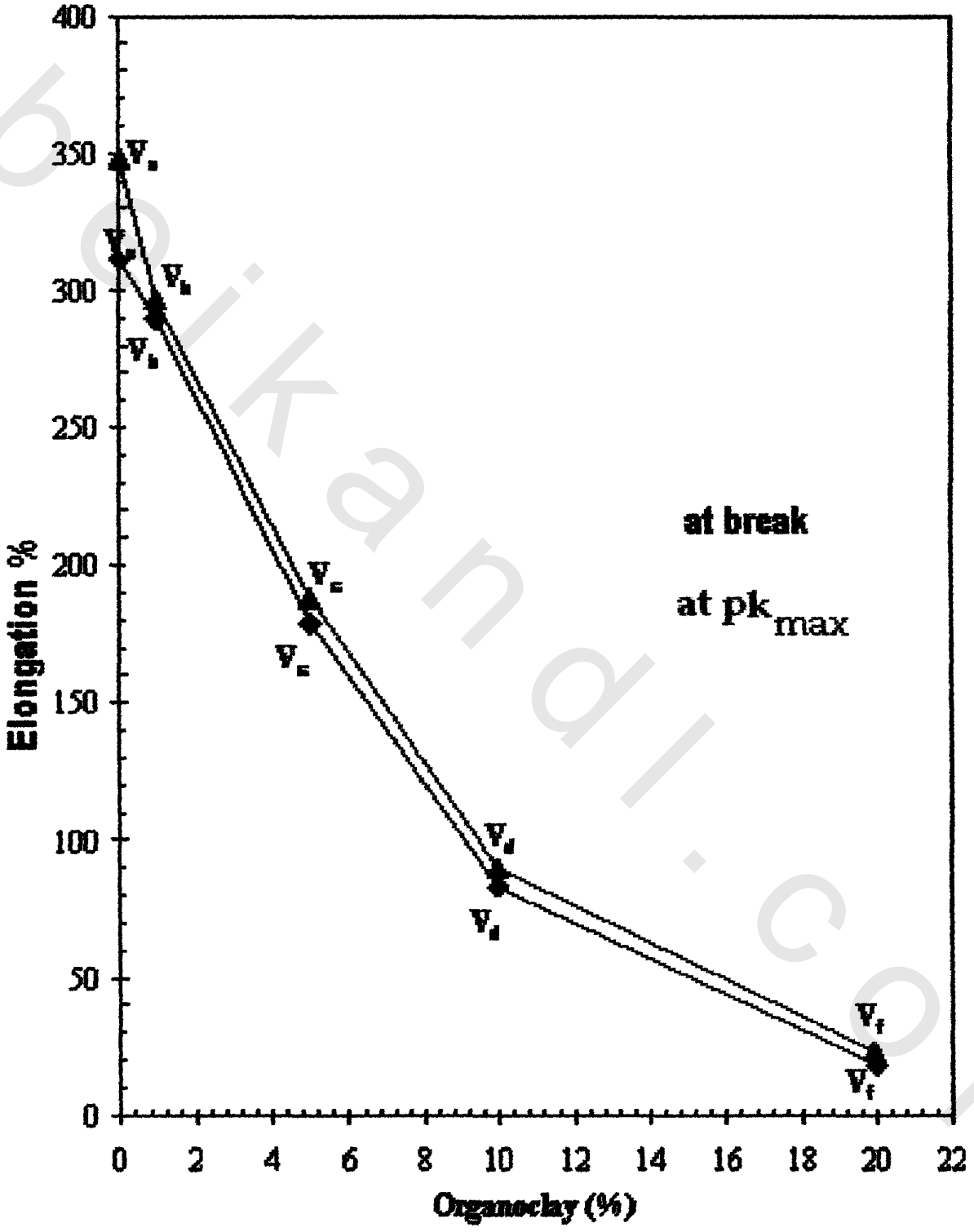

Figure 20: Elongation versus organoclay content for PU/ SMA-ALA-MMT nanocomposites (V_{a-f}) at pKmax and at break.

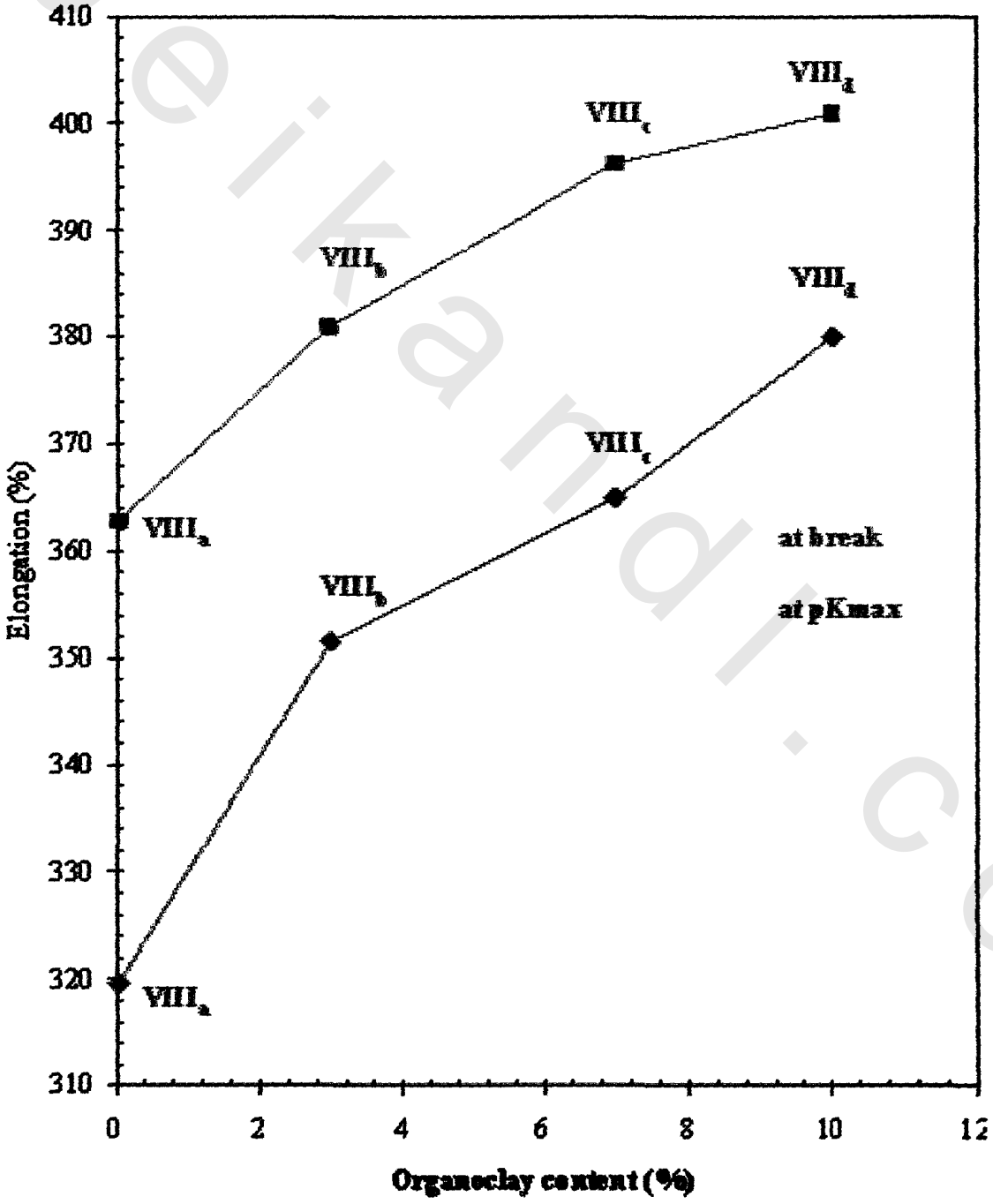

Figure 21: Elongation versus organoclay content for PU/ vinyl monomer-MMT nanocomposites (**VIII$_{a-d}$**) at pKmax and at break.

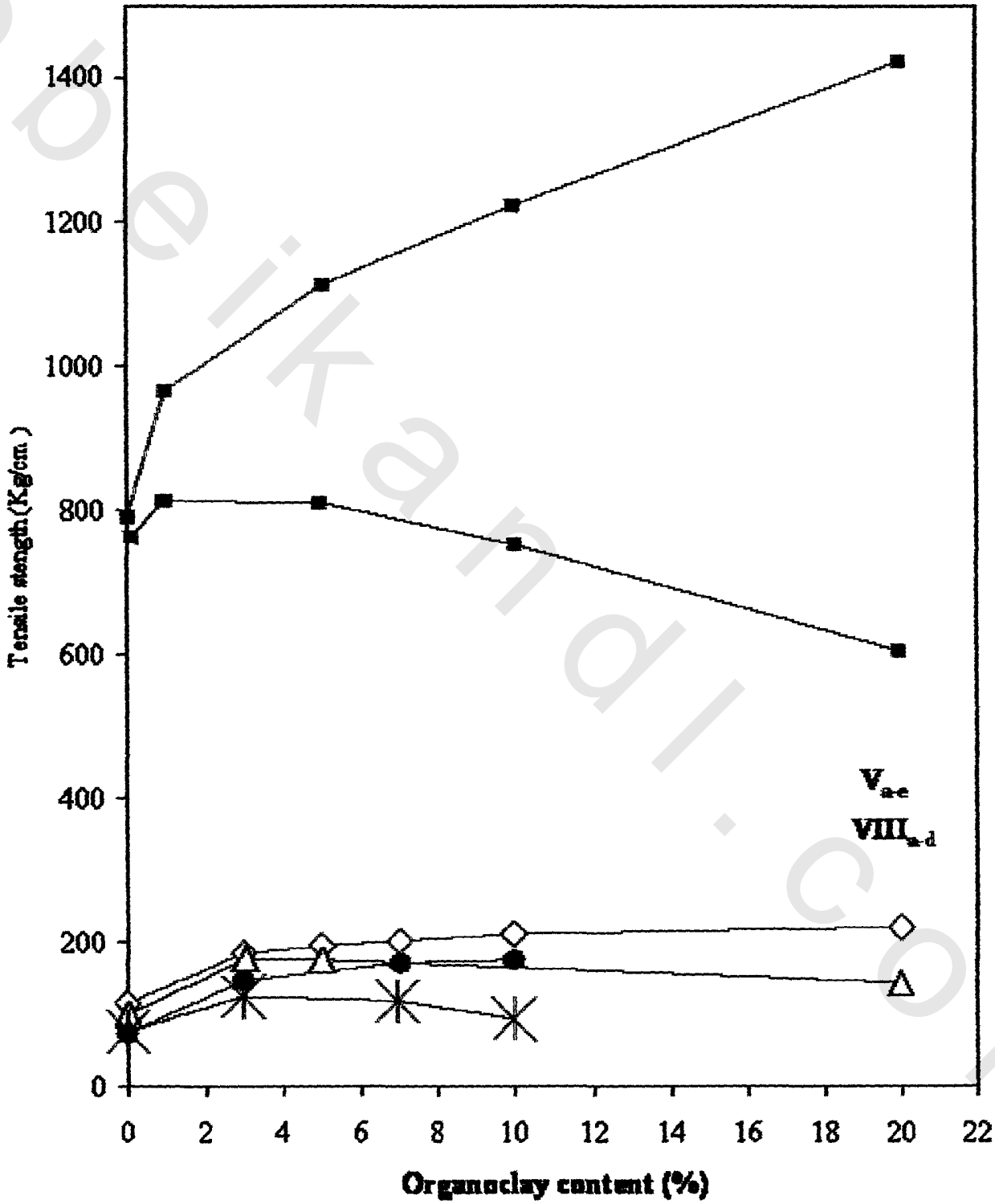

Figure 22: Tensile strength versus organoclay content for PU-organoclay hybrids at pKmax (——) and at break (——)

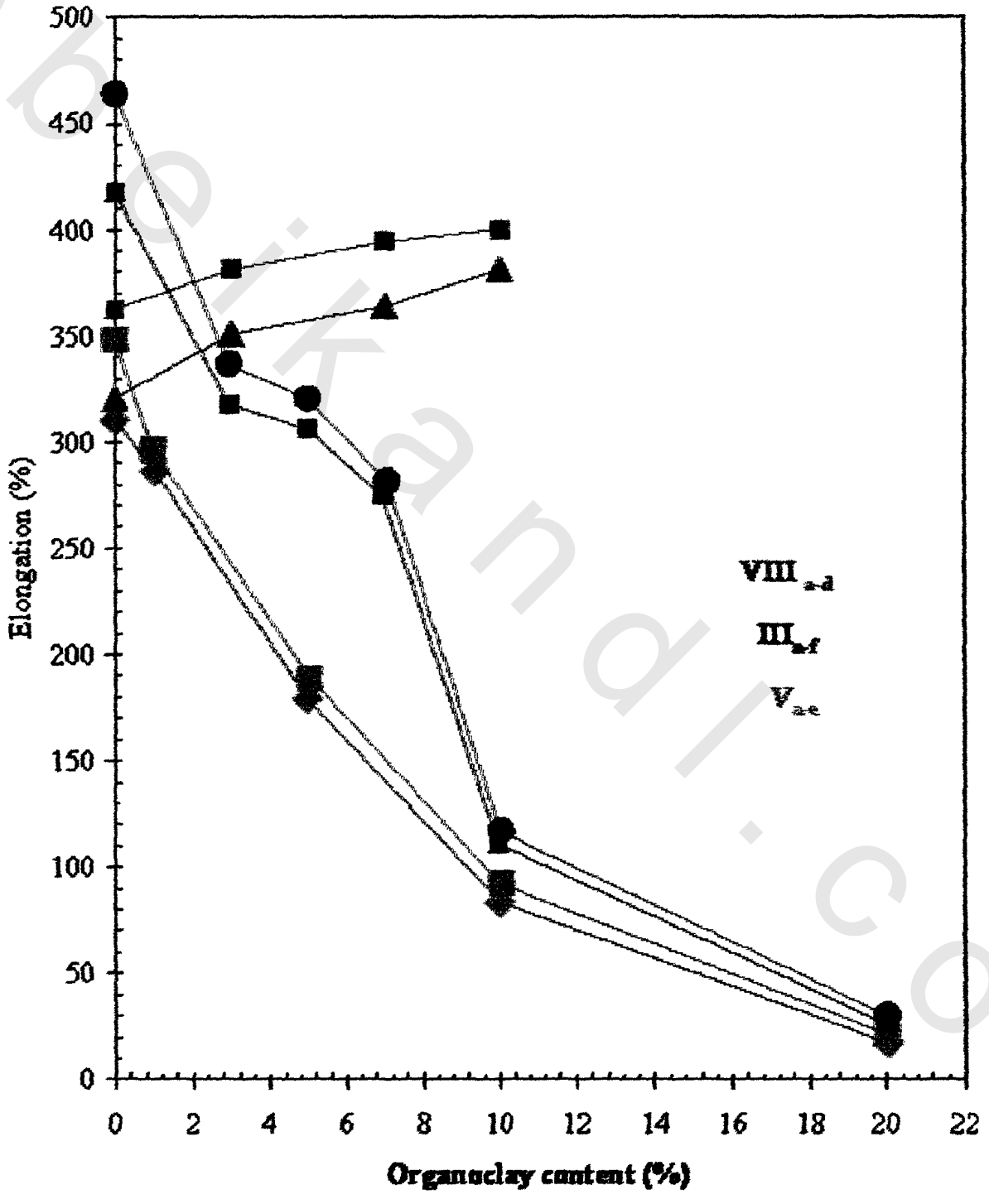

Figure 23: Elongation versus organoclay content for PU- organoclay hybrids at pKmax (——) and at break (—·—)

Table 6: Mechanical properties data for PU/Tyr-MMT nanocomposites films $\mathbf{III_{a-f}}$.

Sample	Organoclay	Thickness	Load Cell (M. Pa)		Tensile Strength (Kg/cm^2)		Elongation (%)	
	$\mathbf{I_a}$ (Wt-%)	μm	At PK_{max}	At Break	At PK_{max}	At Break	At PK_{max}	At Break
$\mathbf{III_a}$	00	430	2.45	2.3	114	107.0	416.5	466.2
$\mathbf{III_b}$	3	390	3.55	3.5	182.1	179.5	318.8	339.9
$\mathbf{III_c}$	5	420	4.08	3.727	194.2	177.5	306.2	321.4
$\mathbf{III_d}$	7	450	4.529	3.785	201.3	168.2	273.4	280.3
$\mathbf{III_e}$	10	400	4.3	3.15	215.0	157.5	110.2	115.6
$\mathbf{III_f}$	20	380	4.2	2.746	221.1	144.7	23.2	25.4

[a] Calculated from the relation

$$\text{Tensile Strength (Kg/cm}^2) = \frac{\text{Force}}{\text{Area (w x t)}} = \frac{\text{M Pa x 10}}{\text{cm}^2}$$

Where w is width and t is thickness of the film under test.

Table7: Mechanical properties data for PU/ SMA-ALA-MMT nanocomposites films $\mathbf{V_{a-e}}$.

Sample	Organoclay $\mathbf{I_b}$ (Wt-%)	Thickness (μm)	Load Cell (M. Pa)		Tensile Strength (Kg/cm^2)[a]		Elongation (%)	
			At PK_{max}	At Break	At PK_{max}	At Break	At PK_{max}	At Break
$\mathbf{V_a}$	00	450	17.708	17.1	787	760	311.8	348.0
$\mathbf{V_b}$	1	380	18.354	15.447	966	813	285.6	296.5
$\mathbf{V_c}$	5	360	19.998	14.598	1111	811	180.0	189.0
$\mathbf{V_d}$	10	440	26.91	16.5	1223	750	84.1	90.0
$\mathbf{V_e}$	20	330	23.55	9.95	1427	603	18.2	23.5

[a] Calculated from the relation

$$\text{Tensile Strength (Kg/cm2)} = \frac{\text{Force}}{\text{Area (w x t)}} = \frac{\text{M Pa x 10}}{\text{cm}^2}$$

Where w is width and t is thickness of the film under test.

Table 8: Mechanical properties, data for PU-Organoclay nanocomposites films **$VIII_{a-d}$**

Sample	Organoclay	Thickness µm	Load Cell (M. Pa)		Tensile Strength (Kg/cm^2)		Elongation (%)	
			At PK_{max}	At Break	At pK_{max}	At Break	At pK_{max}	At Break
	I_c (Wt-%)							
$VIII_a$	00	380	1.524	1.379	80.2	72.6	320	363
$VIII_b$	3	410	2.995	2.64	146.1	128.6	351.5	381
$VIII_c$	7	390	3.31	2.34	169.8	120.2	364.8	396.2
$VIII_d$	10	460	4.08	2.118	177.3	92.1	380.1	401

[a] Calculated from the relation

$$\text{Tensile Strength (Kg/cm2)} = \frac{\text{Force}}{\text{Area (w x t)}} = \frac{\text{M Pa x 10}}{\text{cm}^2}$$

Where w is width and t is thickness of the film under test.

5. XRD Analysis

XRD is powerful technique to observe the change in the interlayer spacing [141]. **Figures 24-28** show typical **XRD** for **Na-MMT**, organoclays ($\mathbf{I_{a, b,c}}$) and hybrid ($\mathbf{III_{b,d-f}}$, $\mathbf{V_{c-e}}$ &$\mathbf{VIII_{b-d}}$.) [141] **Figure 24** shows XRD of I_a after the first and second treatment indicating that the d_{001} reflection was changed from $2\theta = 7.2^{o}$ to $2\theta = 5.8^{o}$ and the re-treatment had no effect on the d_{001} reflection.. The results of **Figure 25** showed that the d_{001} reflection has a peaks at $2\theta = 5.82°$ for $\mathbf{I_a}$, 4.85° for $\mathbf{I_b}$ and 2.63°, 4.78° for $\mathbf{I_c}$ respectively. The d_{001} spacing was calculated from peak positions using Bragg's law [$d = \lambda/(2\ \mathrm{Sin}\theta)$]. The d-spacing for **Na–MMT** ($2\theta = 7.18°$, d-spacing = 12.34 Å) is increased to 15.20 for $\mathbf{I_a}$, 18.24 Å for $\mathbf{I_b}$; and 33.6, 18.48 Å for $\mathbf{I_c}$. These increments in the interlayer spacing suggest that the increase in interlayer spacing depends on the size of the intercalating agent.

Figures 26-28 present three series of **XRD** pattern for PU-organoclay nanocomposites $\mathbf{III_{b,\ d-f}}$, $\mathbf{V_{c-e}}$ and $\mathbf{VIII_{b-d}}$ containing different ratios of organoclay I_{a-c}. The figures show the disappearance of the peak corresponding to the intercalated organoclay with all the ratios (3, 7 10, and 20%). This indicates that the clay was completely exfoliated and homogenously dispersed in the polyurethane matrix. These results confirm that modified **MMT** with different chemical structures and percentages of clay leads to various degree of the dispersion in the polymer matrix. These results are similar to the one described using another structures in PU nanocomposites [142].

Figure 28 shows **XRD** patterns for a series of PU-organoclay nanocomposites $\mathbf{VIII_{b-d}}$ containing different ratios of organoclay. It illustrates the disappearance of the peaks corresponding to d_{001} in the nanocomposites $\mathbf{VIII_b}$ (3 wt %) indicating the formation of exfoliated

nanocomposites in which the polymer molecules are intercalated into the **MMT** galleries and destroyed the oriented distribution of the **MMT** layers. The figure also shows low intense peak corresponding to d_{001} = 3.68 nm in the samples **VIII$_{c, d}$**, (7, 10 wt-%) contrast with the nanocomposites prepared via *in situ* polymerization where the X-ray patterns show a complete exfoliation of clay. This can be attributed to: i) in the case of *in situ* polymerization, the macromolecules with their giant size make complete exfoliation and/or increase the d-spacing of the clay interlayers to become not detectable, ii) in the case of *solution* polymerization the appearance of peaks due to either the formation of two kinds of composites: one is the intercalated nanocomposites and other is partially exfoliated /intercalated nanocomposites or due to the lack of interlayers symmetrical arrangement of polymer into clay interlayers. The appearance of a strong and sharp peak corresponding to d_{001} for the sample **VIII$_d$** indicates that the ordering in the **MMT** layers was enhanced in the composites. Generally, the figure show that the decreasing of organoclay contents from 10 to 3 %-wt % leads to a decreasing of the peak intensity corresponding to d_{001} and disappearing with the small organoclay (3%-wt).

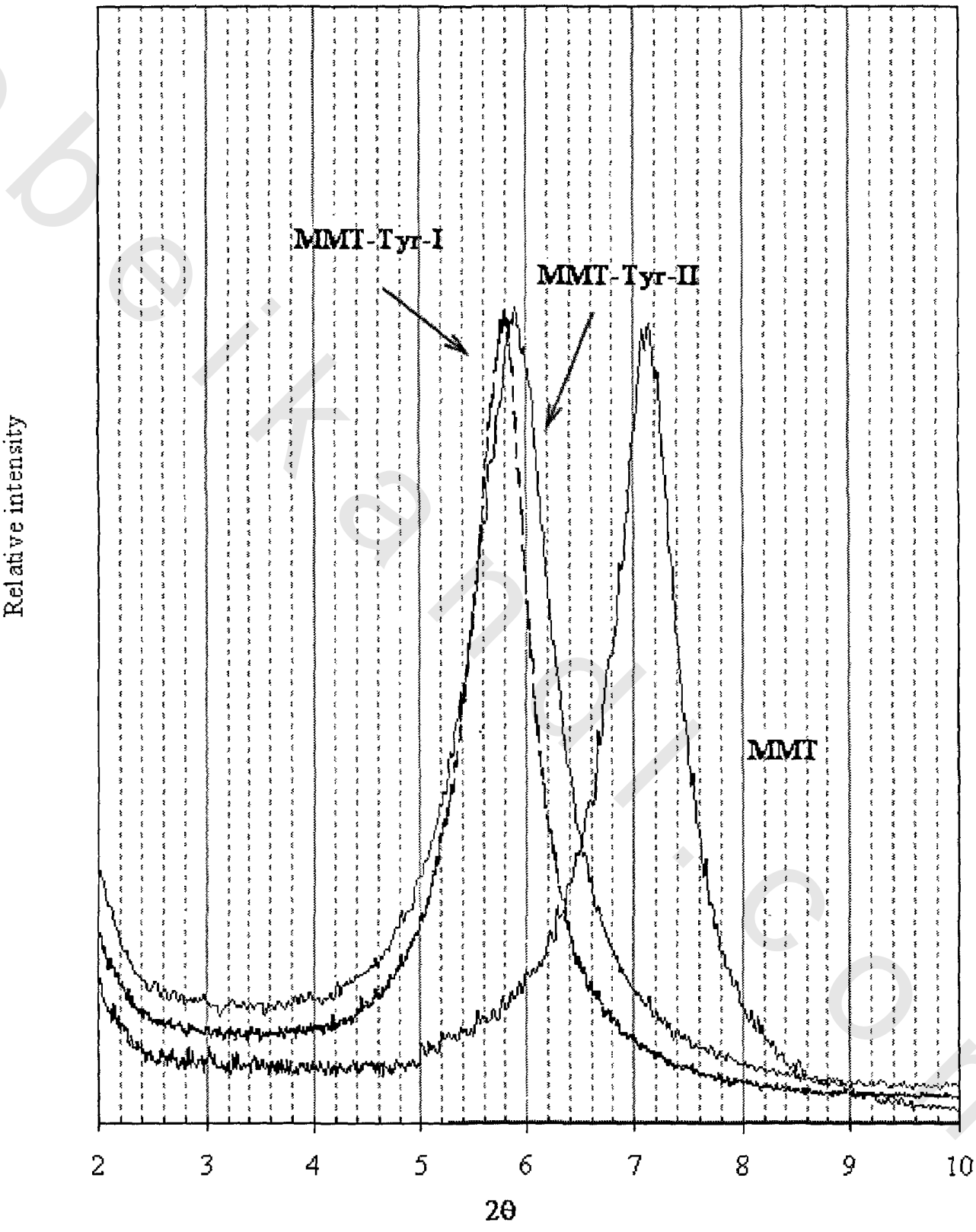

Figure 24 : The X-ray diffraction patterns of Tyr – MMT (I_a)

first and second treatmen

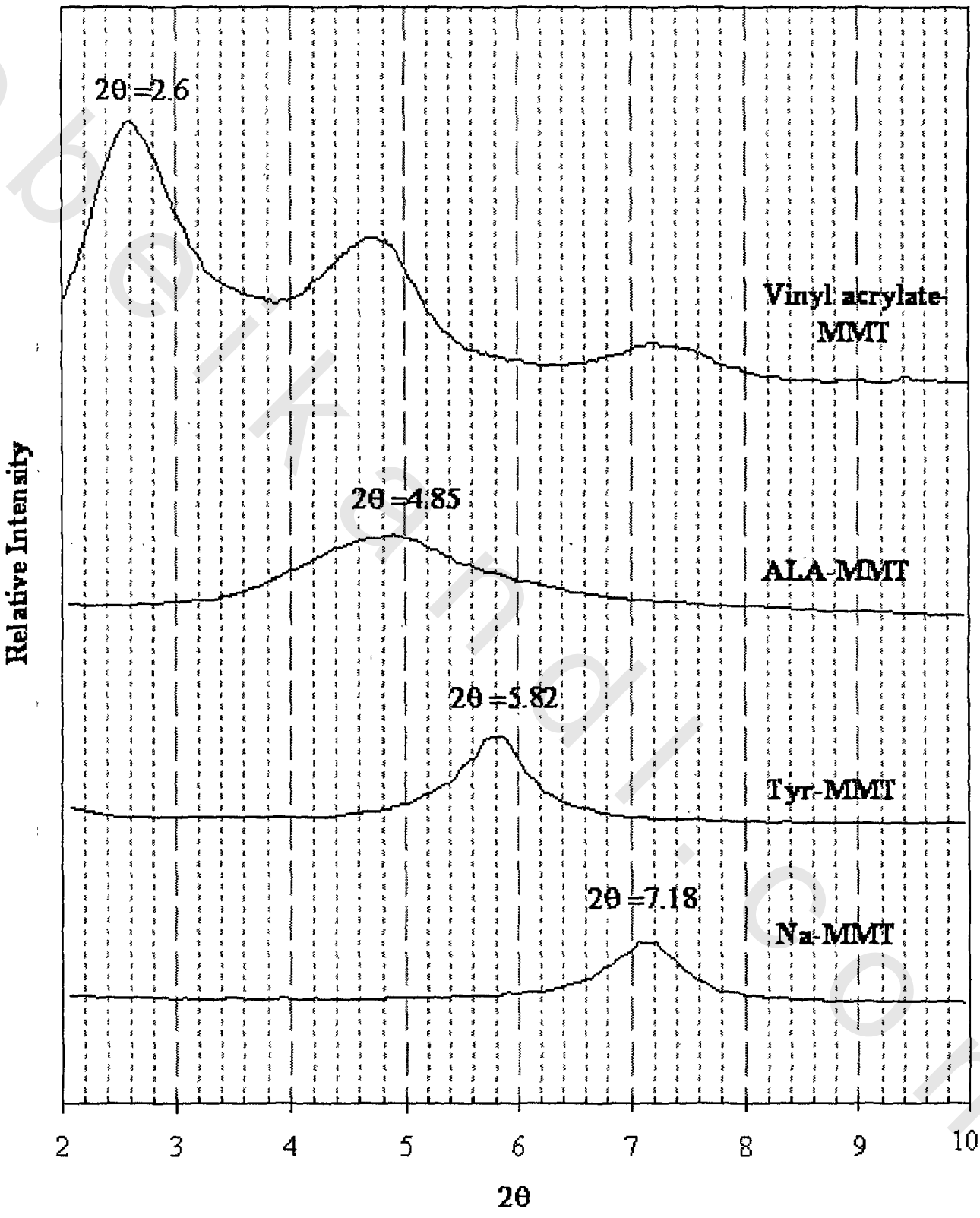

Figure 25: The X-ray diffraction patterns of **Tyr-MMT** (I_a), **ALA-MMT** (I_b), **vinyl acrylate-MMT** (I_c) and **Na-MMT**

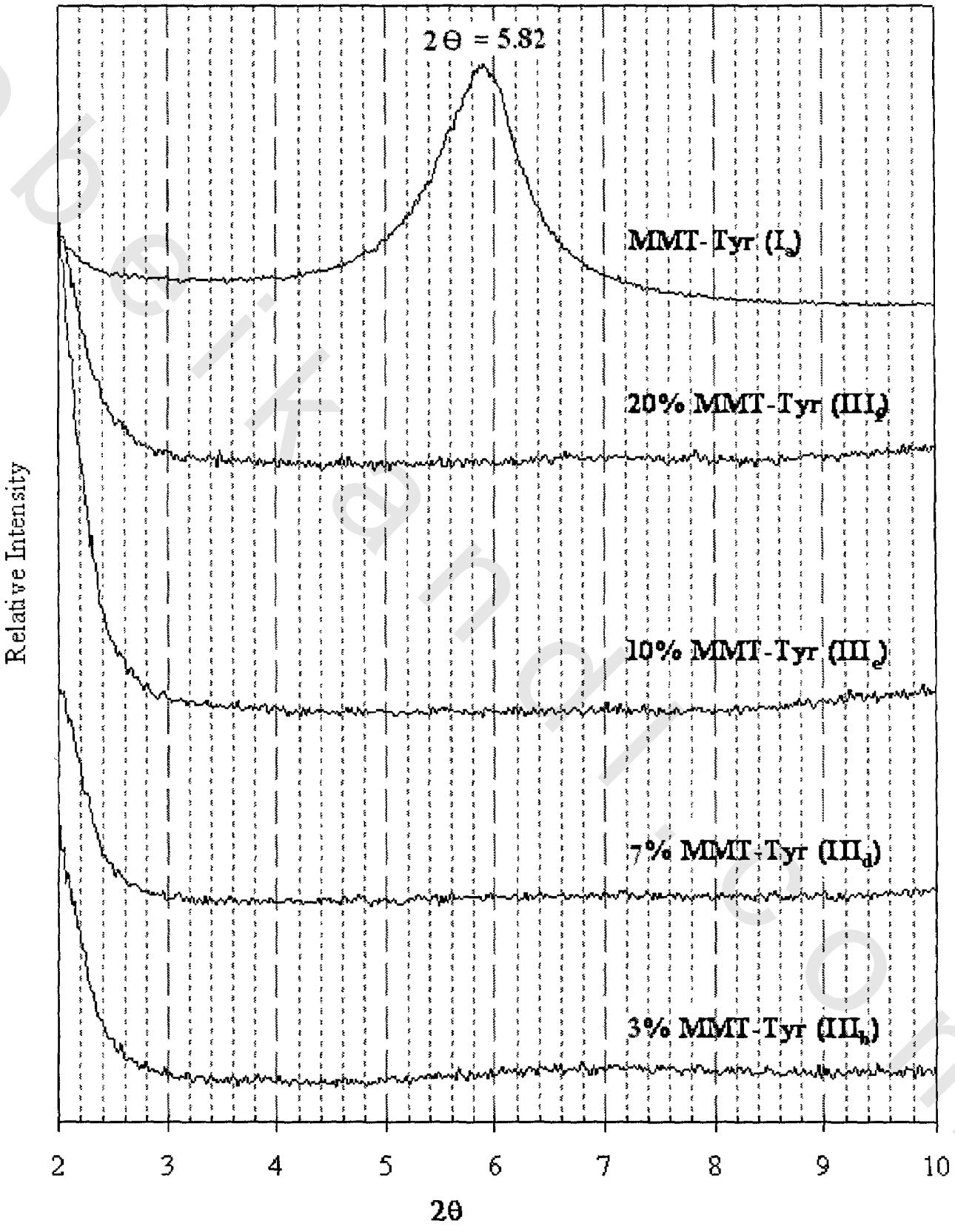

Figure 26: XRD pattern for **Na-MMT**, organoclay **(I_a)** and **$III_{b,d-f}$**

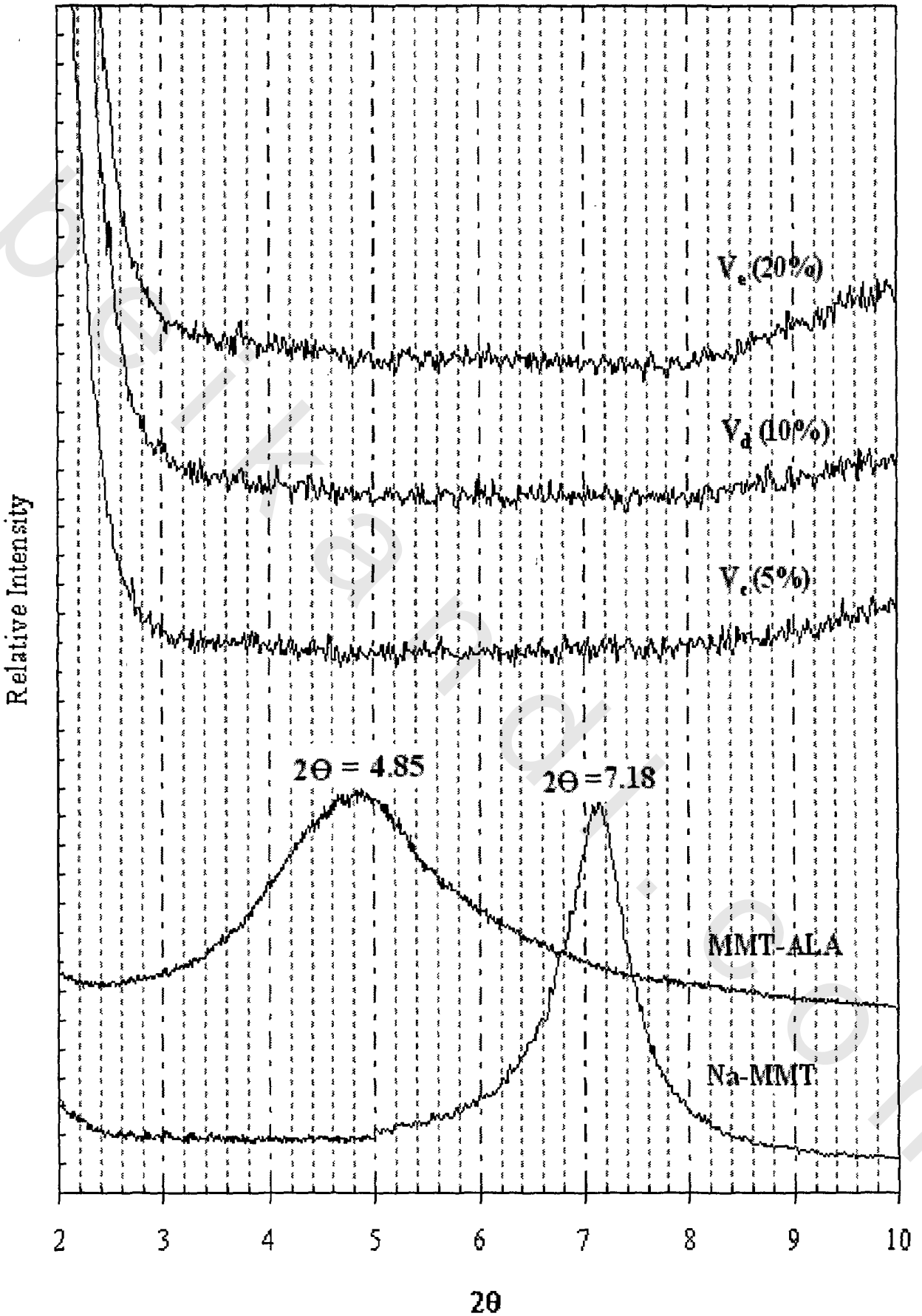

Figure 27: XRD pattern for **Na-MMT**, I_b and $V_{c\text{-}e}$

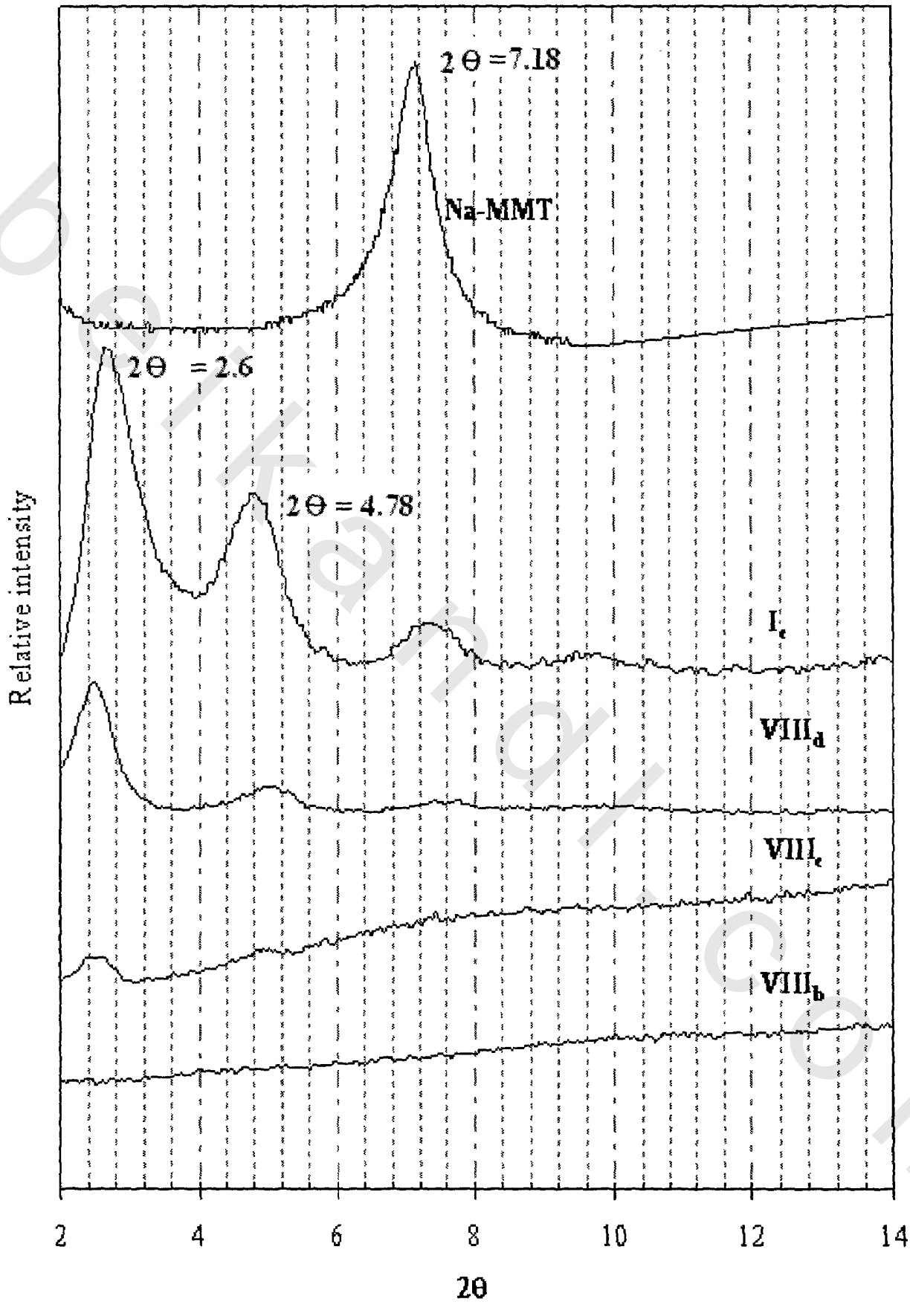

Figure 28: XRD pattern for **Na-MMT, I$_e$ and VIII$_{b-d}$**

6. SEM Results

The morphology of the prepared hybrids was investigated by examination of the surface of the hybrid samples with scanning electron microscope **(SEM).** The micrographs indicate that the PU is intercalated in the interlayer of MMT in a homogenous manner to produce new **PU-MMT** hybrid materials. The micrographs did not show the **MMT** particles on the micron level. **Figures 29-36** show micrographs of the surface at different magnifications for the samples $\mathbf{III_{b\text{-}e}}$, $\mathbf{V_{C,\ e}}$ and $\mathbf{VIII_{b,\ d}}$. The absence of **MMT** particles in the micron level indicates that the agglomerates do not reveal the inorganic domains at the possible magnification. The particle size of **MMT** (0.1-10 μm) is not visible due to well adherent to the polymer and the size of particle is below the resolution of **SEM.** This indicates that the mineral domains are submicron and homogenously dispersed in the polymer matrix. It also, indicates that the polymer was intercalated into the interlayer of **MMT** in a homogenous manner to produce new PU-organoclay nanocomposite materials.

Also, the absence of **MMT** aggregates was confirmed by an energy dispersion x-ray probe. An image for elemental mapping for Silicon **(Si)** was shown in **Figures 29b, 31b,** in which the white dots represent uniformity dispersion of **Si** element. The Silicon mapping shows that the mineral domains are homogenously dispersed in the polymer matrix.

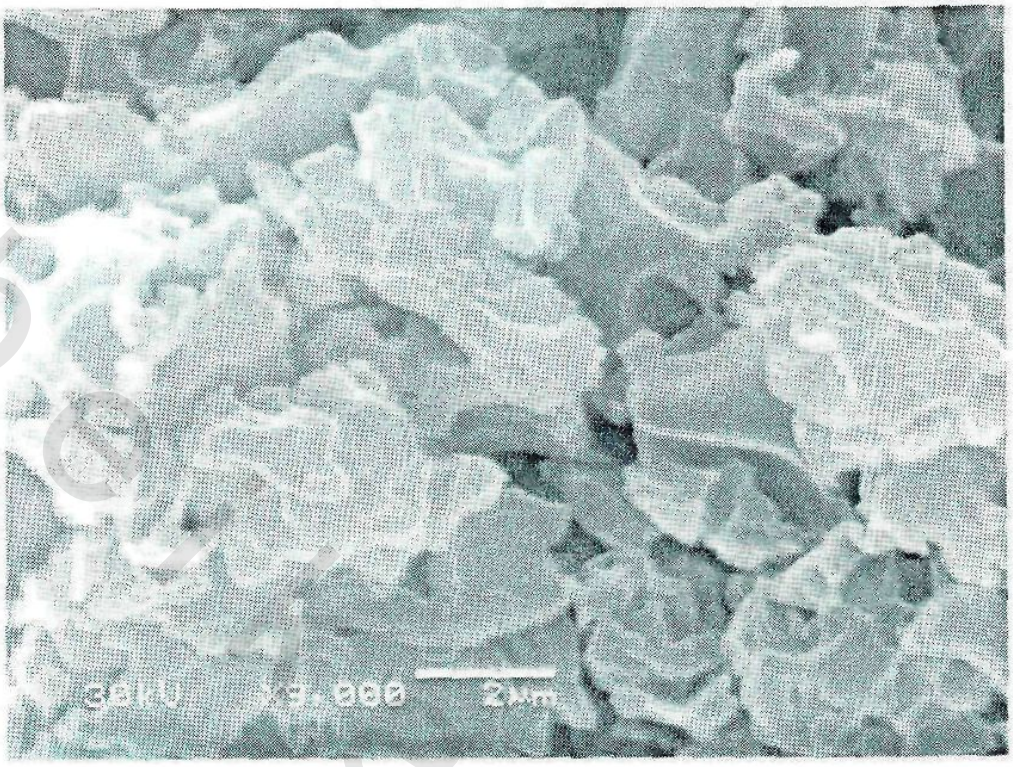

Figure 29a: SEM micrograph for PU/ Tyr-MMT, 3wt. % ($\mathbf{III}_b$)

Figure 29b: Elemental mapping for Si of PU/Tyr-MMT nanocomposite 3 wt. % (III_b)

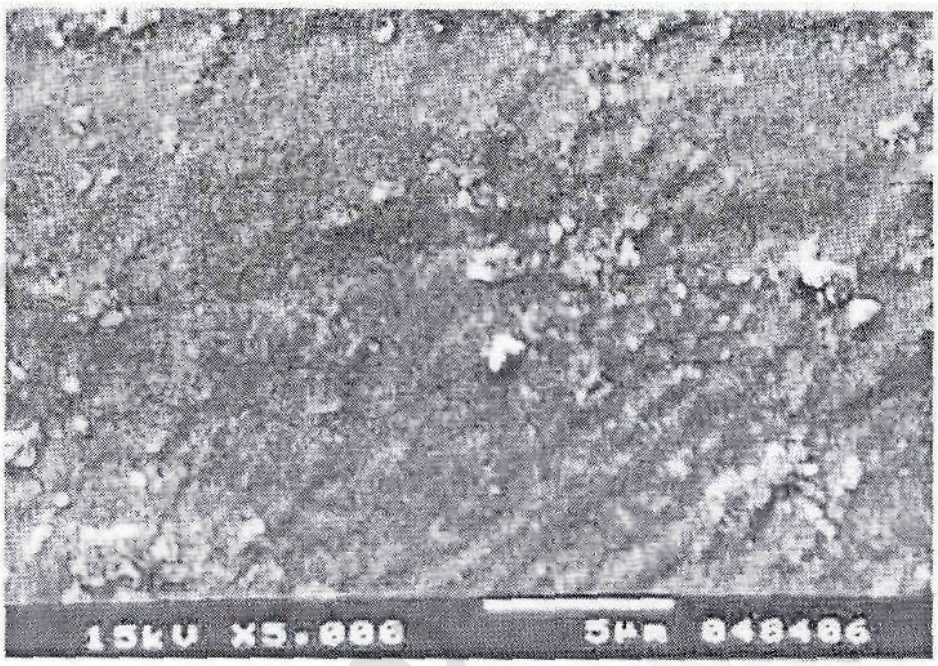

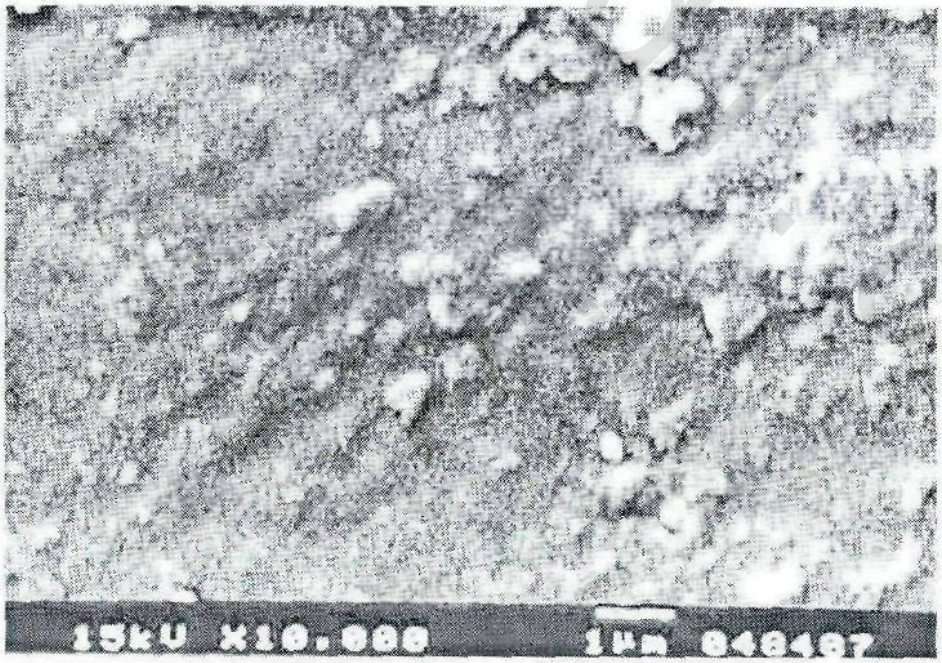

Figure 30: SEM micrograph for PU/T yr-MMT nanocomposite 5 wt. % (IIIc) **at** different magnifications

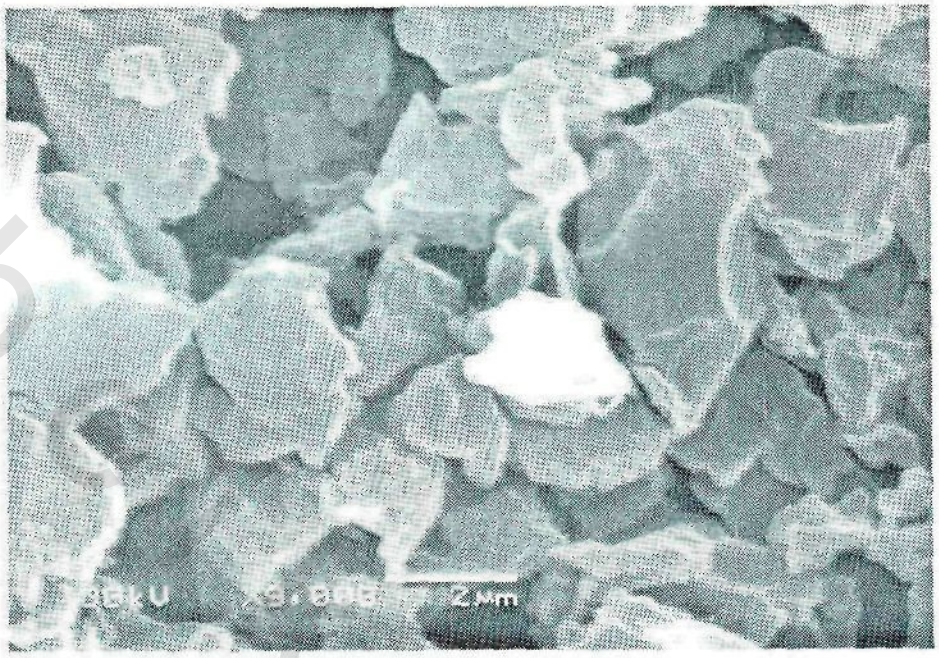

Figure 31a: SEM micrograph for PU/Tyr-MMT, 7 wt. % (IIId).

Figure 31b: Elemental mapping for Si of PU/Tyr-MMT, 7 wt. % nanocomposite ($\mathbf{III_d}$)

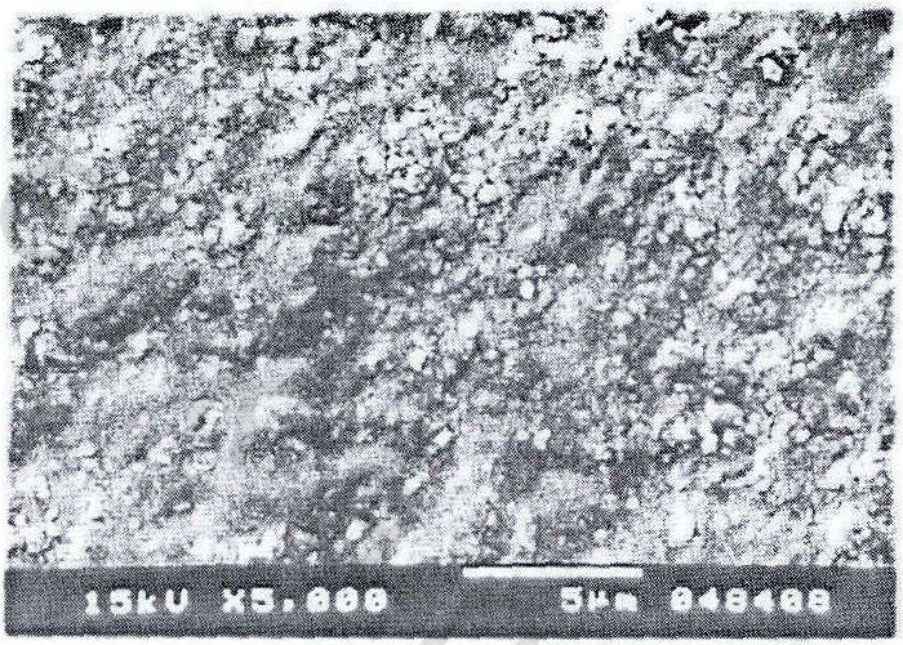

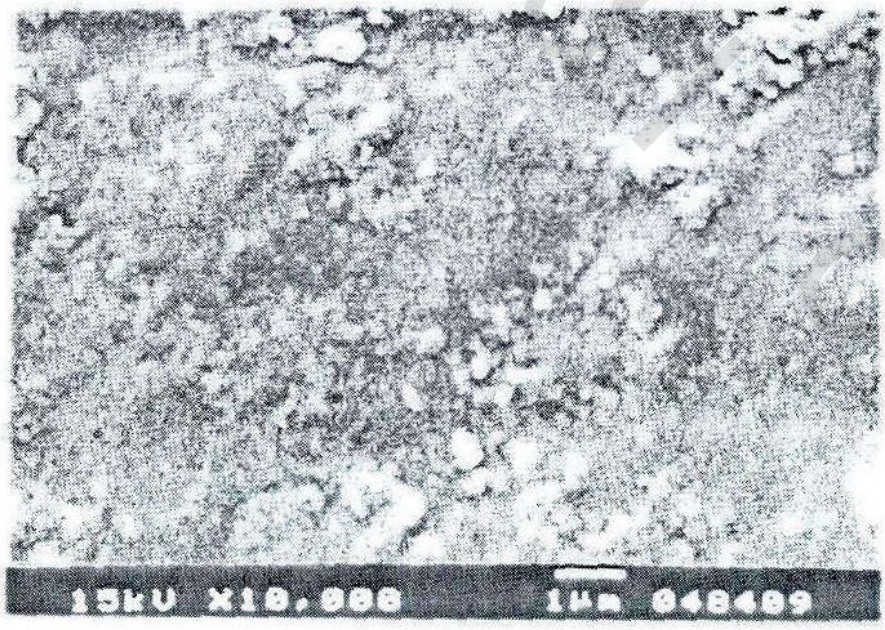

Figure 32: SEM micrograph for PU/Tyr-MMT, nanocomposites, 10 wt. % (IIIe) at different magnification1

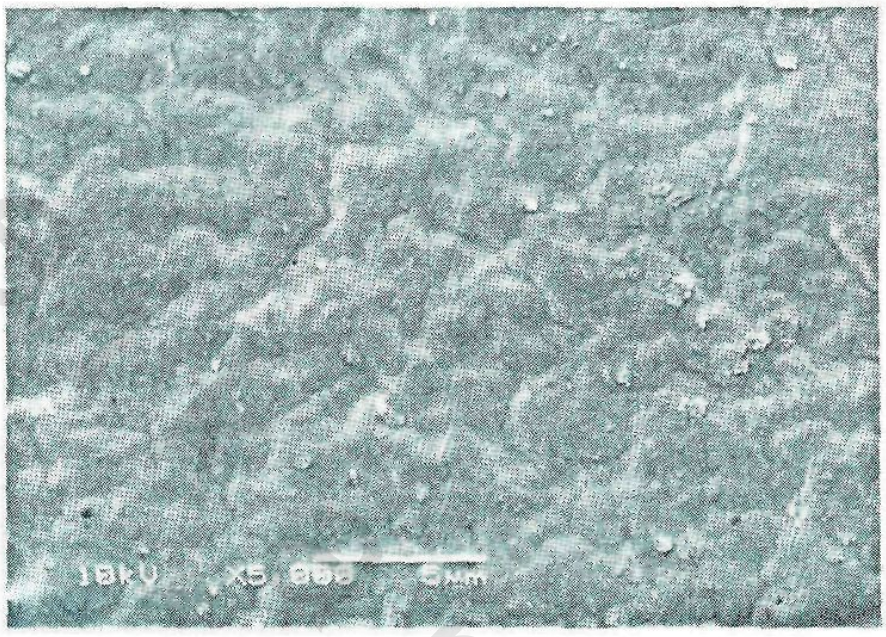

Figure 33a: SEM image of PU/ SMA- ALA-MMT, 5 wt % (V_c)

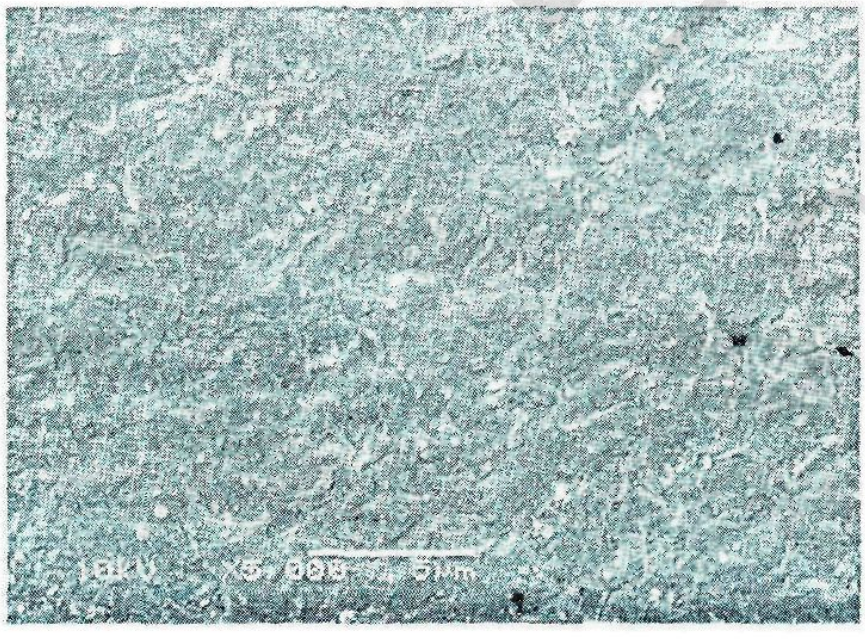

Figure 33b: SEM micrograph of PU/ SMA- ALA-MMT, 10 wt. % (V_d)

Figure 34: SEM micrograph of 20% PU- SMA-ALA-MMT (V_e) at different magnifications

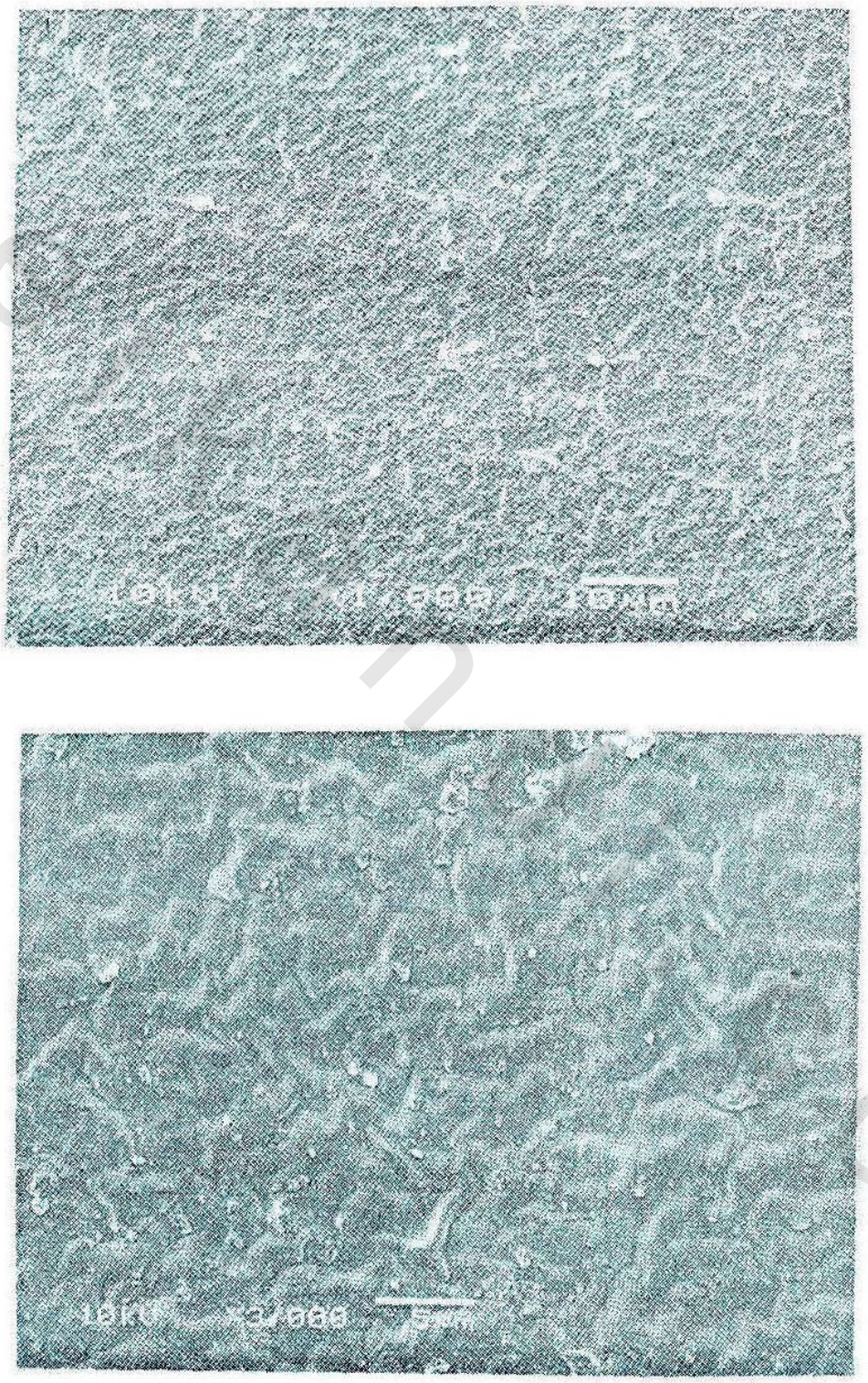

Figure 35: SEM micrograph of PU/ vinyl monomer-MMT, 3 wt. % (VIII $_b$) at different magnification

Figure 36: SEM micrograph of VII_d at different magnification